

# Renormalization group flow, competing phases, and the structure of superconducting gap in multi-band models of Iron based superconductors

Saurabh Maiti, Andrey V. Chubukov

*Department of Physics, University of Wisconsin, Madison, Wisconsin 53706, USA*

(Dated: November 1, 2018)

We perform an analytical renormalization group (RG) study to address the role of Coulomb repulsion, the competition between extended s-wave superconducting order ( $s_{\pm}$ ), and the spin density wave (SDW) order and the angular dependence of the superconducting gap in multi-pocket models of Iron based superconductors. Previous analytic RG studies considered a toy model of one hole and one electron pocket. We consider more realistic models of two electron pockets and either two or three hole pockets, and also incorporate angular dependence of the interactions. In a toy 2-pocket model, SDW order always wins over  $s_{\pm}$  order at perfect nesting;  $s_{\pm}$  order only appears when doping is finite and RG flow extends long enough to overcome intra-pocket Coulomb repulsion. For multi-pocket models, there are two new effects. First, in most cases there exists an attractive component of the interaction in  $s_{\pm}$  channel no matter how strong intra-pocket repulsion is, such that the system necessary becomes a superconductor once it overcomes the competition from the SDW state. Second, in 4-pocket case (but not in 5-pocket case),  $s_{\pm}$  order wins over SDW order even for perfect nesting, if RG flow extends long enough, suggesting that SDW order is not a necessary pre-condition for the  $s_{\pm}$  order. Our analytic results are in full agreement with recent numerical functional RG studies by Thomale et al. [arXiv:1002.3599v1]

## I. INTRODUCTION

Since 2008 a lot of efforts in condensed-matter community have been devoted to solve the puzzle of high- $T_c$  superconductivity (SC) in newly discovered Fe-based superconductors. To a large extent, in two years the community managed to obtain the data for the pnictides in the amount comparable to that collected for the cuprates over twenty years<sup>1</sup>.

The family of Fe-based superconductors is already large and keeps growing. It includes doped 1111 systems  $RFeAsO$  ( $R$  = Rare earth element)<sup>2-5</sup>, doped 122 systems  $XFe_2As_2$  ( $X$ =alkaline earth metals)<sup>6-8</sup>, as well as 111 and 11 systems like  $LiFeAs$ <sup>9</sup> and  $FeTe/Se$ <sup>10</sup>. The parent compounds of most of these materials exhibit a spin density wave (SDW) order<sup>11</sup>, and superconductivity emerges upon either hole or electron doping, or upon gradual substitution of one pnictide by the other ( $As$  by  $P$ ). In some systems, like  $LiFeAs$ <sup>9</sup> and  $LaFePO$ <sup>12</sup>, SC was found already without doping, instead of a magnetically ordered state.

ARPES<sup>13</sup>, de-Haas van Alphen oscillations measurements<sup>14</sup>, and first-principle calculations<sup>15-17</sup> all show that low-energy electronic structure of pnictides in 2D basal plane consists of two nearly circular, non-equivalent hole pockets located at the center of the Brillouin zone(BZ), and two symmetry-related elliptical electron pockets, located near the corners of the BZ in the folded zone scheme, or near  $(0, \pi)$  and  $(\pi, 0)$  points, respectively, in the unfolded zone scheme. [Folded and unfolded zones differ in treating the pnictides – folded zone takes into account the fact that there are two non-equivalent positions of pnictides above and below Fe plane, and has two Fe atoms in the unit cell, while unfolded zone incorporates only Fe atoms and has one Fe atom in the unit cell.] These hole and electron pockets form warped cylin-

ders in 3D space. In addition, in some pnictides there is a fifth cylindrical hole pocket centered at  $(\pi, \pi)$  in the unfolded zone (at  $(0, 0)$  in the folded zone, like other two hole pockets), while in other pnictides this fifth Fermi surface (FS) becomes a 3D sphere centered near  $k_z = \pi$  along  $z$ -direction.

A lot of work has been done over the last two years regarding the symmetry of the order parameter and the interplay between SDW and SC orders. Most of researchers (but not all, see Ref. 18) believe that the gap symmetry is extended  $s$ -wave ( $s_{\pm}$ ), meaning the gap transforms according to  $A_{1g}$  representation of  $D_{4h}$  tetragonal symmetry group, but the average gap values along hole and electron Fermi surfaces have different sign. However, the structure of the gap is still a puzzle. Early works based on either spin-fluctuation scenario<sup>17,19-21</sup> or on renormalization group (RG) study of a toy model of one hole and one electron FS<sup>22,23</sup> found a simple angle-independent  $s_{\pm}$  gap. Subsequent more sophisticated numerical studies, which take into account multi-orbital nature of low-energy excitations in the pnictides, have reported angular dependence of the  $s_{\pm}$  gap, with  $\cos 2\phi$  variations on the electron FSs and  $\cos 4\phi$  variations along the hole FSs<sup>20,24-27</sup>. The  $\cos 2\phi$  modulations of the  $s_{\pm}$  gap on the electron FSs has also been obtained in the analytical study<sup>28</sup>. If  $\cos 2\phi$  variation is strong enough, the gap has “accidental” nodes along electron FSs, still preserving  $s_{\pm}$  symmetry.

Other recent theory proposals include  $s^{++}$  state<sup>18</sup>,  $s_{\pm}$  state with nodes on hole FSs due to strong  $\cos 4\phi$  modulations<sup>29</sup>, and  $s^{+-}$  state with nodes at particular  $k_z$  along  $z$ -direction<sup>30</sup>.

Experiments are generally consistent with  $s_{\pm}$  gap symmetry, but whether or not the gap has nodes in particular materials is still subject of debate<sup>31-43</sup>. In addition, there is no information yet from the experiments where the gap

nodes are located, if present. ARPES measurements of the gap along hole FSs (taken at fixed  $k_z$ ) on various  $Fe$ -pnictides<sup>44–46</sup> indicate that the gap is almost angle independent, but the detailed measurements of the gap separately along each of the two electron FSs are still lacking, with only few exceptions<sup>48</sup>.

From theoretical perspective, the most relevant issue is the nature of the pairing interaction. Conventional electron-phonon coupling is always a candidate, particularly when the gap has  $s$ -wave symmetry, but has been shown to be rather weak<sup>16</sup>, and is incapable to account for  $T_c \sim 50K$  even if one neglects destructive effect of Coulomb interaction. This leaves electron-electron interaction (i.e., dressed Coulomb repulsion at a finite momentum transfer) as the dominant pairing interaction. Such interaction cannot give rise to a constant  $s$ -wave gap, but it can give rise to either momentum-dependent, sign reversing gap along a given FS, like  $d_{x^2-y^2}$  gap in the cuprates, or to gaps of different signs along different FSs. Coulomb interaction at large momentum transfer contributes to the pairing both directly and by creating effective pairing interactions mediated by collective excitations in either spin or charge channel. The close proximity to magnetism makes spin fluctuations a preferable candidate<sup>17,19,24</sup>, although orbital fluctuations were also considered recently<sup>47</sup>. Both direct Coulomb interaction (the pair hopping) and magnetically-mediated interaction are attractive for  $s\pm$  gap, and the total attractive pairing interaction is a combination of the two. Still, to give rise to a pairing, this combined attractive pairing interaction has to overcome repulsion coming from Coulomb interaction at small momentum transfers. A conventional McMillan-Tolmachev renormalization<sup>49</sup> does not help here because both repulsive and attractive parts of the interaction renormalize in the same way, and if repulsive part is initially stronger, the renormalization just reduces the strength of the total repulsive interaction, but cannot change its sign.

How to overcome Coulomb interaction became the major issue for  $s$ -wave pairing in the pnictides. The situation is further complicated by the fact that low-energy excitations are composed of all 5 hybridized  $Fe$  3d-orbitals, and Coulomb interactions between fermions belonging to a given orbital and belonging to different orbitals are equally important. Only if all of these interactions are approximated by the same momentum-independent Hubbard  $U$ , this  $U$  cancels out in the pairing problem and one is left with a pure spin-mediated interaction (this was termed “Coulomb avoidance”<sup>50</sup>). In reality, Coulomb interaction is momentum-dependent and is larger at a small momentum transfer than at a large momentum transfer, and intra-orbital and inter-orbital interactions are also different. As a result, direct Coulomb pairing interaction is repulsive for superconductivity with angle-independent plus-minus gap. Spin-mediated interaction is attractive and can potentially compete with direct Coulomb repulsion. However, at least at weak/moderate coupling direct Coulomb repulsion is the largest term. This holds even

when magnetic correlation length  $\xi$  diverges because for the pairing one generally needs the interaction at non-zero frequencies, where it remains finite.

There are two possibilities to obtain  $s\pm$  superconductivity despite strong Coulomb repulsion. First, multi-orbital character of excitations in the pnictides implies that the attractive pairing interaction (either pair hopping or spin-fluctuation exchange) is angle-dependent. The angle-dependence comes from coherent factors which dress up the interactions when one transforms from the orbital picture -in which different parts of the Fermi surface are made of different orbitals- to the band picture, in which free-fermion part is simply  $\epsilon_k c_k^\dagger c_k$ , and all information about multi-orbital character is passed onto interactions. Once interaction is angle-dependent, the gap also becomes angle-dependent, and the system adjusts the angle-dependence of the gap to minimize the effect of Coulomb repulsion (we discuss this in more detail below). The most natural is the case when the gap acquires  $\pm \cos 2\phi$  components along the two electron FSs, and the magnitude of this component is adjusted to balance the interplay between small  $q$  Coulomb repulsion and the combined attractive interaction in  $s\pm$  channel. When Coulomb repulsion dominates, the angle-dependent part is large, and the gap has four nodes along each of the electron FSs.

Second, one can analyze how the interactions evolve as the system flows towards smaller energies, relevant to superconductivity. This flow involves renormalizations of interactions in both particle-hole(p-h) and particle-particle(p-p) channel, and goes beyond RPA. This flow has been studied numerically, using functional renormalization group (fRG) technique<sup>25–27</sup> and analytically<sup>22,28,51</sup>, within parquet RG. Both are weak-coupling studies, based on the Hamiltonian which contains screened Coulomb interaction, but no additional spin-fluctuation interaction. The results of both types of studies are quite similar: it turns out that Coulomb repulsion at small momentum transfers decreases upon system flow to smaller energies, but the pairing interaction at large momentum transfers (the pair-hopping from hole to electron FSs), which is attractive for  $s^{+-}$  superconductivity increases. The increase of the pair hopping is the result of the “push” from the inter-pocket density-density interaction which by itself leads to SDW instability. If RG flow of the couplings persists over a wide enough range of energies, pair-hopping interaction exceeds Coulomb repulsion, and the system develops an attraction in the  $s\pm$  channel. In this situation, the  $\pm \cos 2\phi$  variations of the gap on electron FSs induced by angle dependence of the interaction, are not crucial for the pairing, and the system can develop an  $s\pm$  gap without nodes.

While this scenario is quite generic, the earlier parquet RG study<sup>22,51</sup> was more limited in scope. It was done for a toy model of one hole and one electron FS centered at  $(0,0)$  and  $(\pi,\pi)$ , respectively. For such a model, angle dependencies of the interactions must be symmetric with

respect to interchanging  $x$  and  $y$  momentum components both near  $k = (0, 0)$  and  $k = (\pi, \pi)$  and can only be in the form  $\cos 4\phi$ ,  $\cos 8\phi$ , etc which are subleading terms in the expansion of  $A_{1g}$  gap for a single FS (no  $\cos 2\phi$  terms!). Such  $\cos 4n\phi$  terms are generally irrelevant and were neglected in toy model analysis, i.e. the gap along each of the FSs was approximated by a constant. Like we said, for momentum-independent gaps, the bare interaction in the  $s^{+-}$  channel is repulsive if intra-pocket Coulomb repulsion is the largest. The interaction flows under RG and changes sign at some value of RG parameter. Still, all along parquet RG flow, the pairing interaction remains secondary to the interaction in the SDW channel. As a result, for perfect nesting the system develops an SDW order. Only when the system is doped and the logarithmical flow of the SDW vertex is cut at low energies, SC channel takes over and the system develops an  $s^{+-}$  superconductivity.

In the present paper we extend earlier parquet RG analysis to multi-pocket models of Fe-pnictides. We consider two models. The first one has two electron FSs, located at  $(0, \pi)$  and  $(\pi, 0)$  in the unfolded zone, and two hole FSs located near  $(0, 0)$ . The second model has an additional hole pocket centered at  $(\pi, \pi)$  in the folded zone. The presence or absence of this additional FS in different Fe-pnictides is attributed<sup>19,27</sup> to the difference in the distance between the pnictide (e.g.,  $As$  or  $P$ ) and the Fe-plane. To avoid overly complicated analysis of RG equations we only consider two limiting cases: one when the two hole pockets centered at  $(0, 0)$  are completely equivalent, and the other when one pocket is coupled to electron FSs much weaker than the other one and can be neglected [this effectively reduces 4 pocket model to 3 pockets and 5-pocket model to 4 pockets]. The system behavior is identical in the two limits which gives us confidence that it remains the same also in between the limits. Throughout the paper we assume that all FSs are cylindrical and neglect their variations along  $k_z$ .

We argue that new physics: nodal  $s^\pm$  SC, appearance of SC even at perfect nesting, emerges once one extends the model from 2 to 4 pocket (or to 3-pocket when only one hole FS is relevant). This result is consistent with early assertions<sup>22,28</sup> that the 3-pocket model is the minimum model needed to understand the key physics of  $Fe$ -pnictides. The behavior of 5 pocket model, on the contrary, is in many respects similar to that for 2-pocket model (except that nodal  $s^{+-}$  SC is still possible). That 4-pocket and 5-pocket models behave differently under RG has been the conclusion of fRG study by Thomale *et al* (Ref.27), and our results fully agree with their analysis.

We extend previous 2-pocket study in two directions. First, we incorporate  $\cos 2\phi$  angular dependence of the interactions which give rise to  $\pm \cos 2\phi$  modulations of the gaps on electron FSs. In this situation, there are at least three different effective vertices for  $s^\pm$  gap symmetry, and we argue that, if the dominant angle dependence comes from electron-hole interaction, one of them remains positive (i.e., attractive) over the entire RG flow even when

bare intra-pocket repulsion is the largest interaction. We show that the stronger is the angular dependence of the interaction, the stronger is the tendency to develop an nodal  $s^\pm$  order.

Second, we re-analyze the interplay between SC and SDW channels. For angular-dependent interactions, are also several SDW vertices of which at least one is attractive along the whole RG trajectory. We compare the flow of the leading vertices in SDW and SC channel. We show that in 4-pocket model, the trajectory of the leading SC vertex are steeper than that of the leading SDW vertex, and the latter remains larger only down to some RG scale. At smaller scales (i.e., when RG flow extends further to lower energies) the SC vertex overshadows SDW vertex even at perfect nesting. This agrees with fRG study by Thomale *et al.*<sup>27</sup>. We argue, based on our analytic consideration, that the crossing between SC and SDW vertices under RG flow is to a large extent a combinatoric effect – compared to 2-pocket case (where SDW and SC vertices flow to the same value under RG), the presence of the two electron FSs adds the factor of 2 to the renormalization of the SC vertex as the pair hopping can, e.g., hop a pair of  $k, -k$  fermions from the hole FS to each of the two electron FSs, but momentum conservation does not allow such factor of 2 to appear in the renormalization of the SDW vertex.

We further find that for 5-pocket model, SC vertex always remains secondary compared to SDW vertex, just like in 2-pocket model. Furthermore, like in 2-pocket model, SC and SDW vertices flow to the same value at the fixed point. This again agrees with fRG result by Thomale *et al.*

The rest of the paper is organized as follows: Section II outlines our approach, explains the subtleties in the RG flow, and discusses the technique by which we incorporate the momentum dependence into our analysis. In Sec. III we briefly review the results for the 2-pocket case. Section IV is the central section in the paper – here we consider in detail the 4-pocket model. We discuss SC vertices in the presence of angular dependence of the interaction, the RG flow, and the competition between SC and SDW instabilities. Most of our treatment in this section is for the limit when one of the hole FS can be neglected. Later in the section we analyze another limit when the two hole FS are equivalent and show that the system behavior is identical in the two limits. In Sec. V we discuss 5-pocket model and argue that its behavior to a large extent is similar to that in 2-pocket model. We summarize our results in the Conclusion.

## II. DISCUSSIONS

Before starting the detailed description of each model, we present a brief discussion on the outline of our approach. We first describe the central idea behind our analysis, then describe the technique through which we

incorporate the angular dependence of the vertices and finally discuss how we incorporate these into RG equations.

### A. Approach

We consider four-fermion interactions between fermions located close to the FSs of two or more pockets. We consider Hamiltonian with all possible quartic interactions allowed by symmetry and ask what can be said about the onset of SC, SDW, and, possibly, CDW instabilities. The usual approach is to write down equations for effective vertices  $\Gamma_i$  in SDW, SC, CDW channels and check for the existence of critical temperatures  $T_{ins}^{(i)}$  at which  $\Gamma_i$  diverges. In case of competing instabilities, the equations for the effective vertices are coupled and, once the coupled system is solved, the instability with the highest  $T_{ins}(T_c)$  takes over.

As we said in the Introduction, when one does such an analysis, one deals with interactions taken at the scale of  $T_c$ , which are not the same as the terms in the Hamiltonian. To account for the flow of the couplings from the scale of the bandwidth down to  $T_c$ , we need RG analysis. This analysis assumes renormalizability of the theory and can be rigorously justified only when the RG flow is logarithmic (i.e., interactions vary as functions of the logarithm of the running scale  $E$ ). One well-known example of logarithmic RG flow is the renormalization in the particle-particle channel (Cooper renormalization). Another, specific to our case, is the renormalization in the particle-hole channel, involving intermediate fermions from hole and electron pockets. Because hole and electron dispersions are of opposite sign, such a renormalization also generates logarithmic dependence of the running energy and/or momentum as long as the running energy exceeds the sum of energies of the top of the hole band and the bottom of the electron band (hole and electron masses do not have to be equal).

The logarithmic renormalizations in the particle-particle and particle-hole channels are characterized by corresponding polarization bubbles. Let  $c$  describe a hole band centered at  $k = 0$  and  $f$  describe an electron band centered at  $Q$ . Assume for simplicity that hole and electron masses are equal. For a perfect nesting, hole and electron dispersions obey  $\varepsilon_c(k) = \varepsilon_0 - k^2/(2m_h) = -\varepsilon_f(k + Q)$ . The two logarithmically singular polarization bubbles are

$$\begin{aligned}\Pi_{pp}^{cc}(q, \Omega) &= \Pi_{pp}^{ff}(q, \Omega) \\ &= \int \frac{d^2k d\omega}{(2\pi)^3} G^c(k, \omega) G^c(q - k, \Omega - \omega) \\ &= \frac{m}{2\pi} L + \dots \\ \Pi_{ph}^{cf}(q + Q, \Omega) &= \int \frac{d^2k d\omega}{(2\pi)^3} G^c(k, \omega) G^f(q + Q + k, \Omega + \omega) \\ &= -\frac{m}{2\pi} L + \dots \\ L &= \frac{1}{2} \ln \left( \frac{\Lambda}{E} \right)\end{aligned}\tag{1}$$

where the dots stand for non-logarithmic terms,  $E = \max\{\Omega, v_F q\}$  and  $E > E_F$ ,  $\Lambda$  is the upper cutoff of order bandwidth, and the propagators are given by  $G^x = \frac{1}{i\omega - \varepsilon_k^x}$ ,  $x$  being  $c$  or  $f$ .

The RG study requires caution as the couplings flow differently for energy scales above  $E_F$  and below  $E_F$ . The reasoning is simple: logarithmic RG analysis requires that internal momenta in each diagram for vertex renormalization be larger than external momenta, which are of order  $k_F$ . When typical internal energies are larger than  $E_F$ , internal momenta are larger than  $k_F$ , and vertex corrections in both particle-particle and particle-hole channel are logarithmic. This gives rise to parquet RG. When typical energies are smaller than  $E_F$ , the strength of the renormalization in the particular channel depends on the interplay between external momenta. When total incoming momenta is zero, renormalization in the particle-particle channel is still logarithmically singular, but in the renormalization of the particle-hole channel, the logarithm is cut by external  $E_F$ . Conversely, for the vertex with transferred momentum equal to the distance between hole and electron FSs, the renormalization in the particle-hole channel is still logarithmic, but in the renormalization in the particle-particle channel, the logarithm is now cut by external  $E_F$ . As a result, the renormalizations in the particle-particle and particle-hole channels are coupled at energies above  $E_F$ , but become decoupled at energies below  $E_F$ . At  $E < E_F$  parquet RG equations are replaced by conventional ladder RG equations  $d\Gamma_i/dl = \Gamma_i^2$ , where  $l = \log E_F/E$ . Thus the flow of the couplings splits into the flow from the bandwidth down to  $E_F$ , where different vertices are all coupled, and the flow below  $E_F$ , where different vertices are decoupled (see Fig. 1). This reasoning is particularly important in our case, as in pnictides  $E_F \sim 100\text{meV}$  is much smaller than the bandwidth, which is a few electron volts.

Depending on the character of the flow, the bare values of the couplings, and the ratio of the bandwidth and the Fermi energy, several situations are possible and shown in Fig. 2:

- The RG flow diverges and the normal state becomes unstable before the scale of  $E_F$  is reached (Fig. 2a). In this situation, the instability is reached

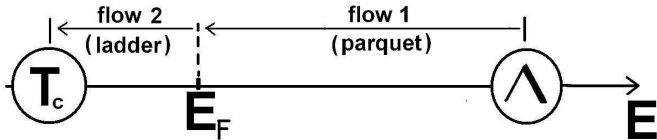


FIG. 1: Illustration showing how the couplings evolve under RG flow. The bare couplings (the parameters of the Hamiltonian) are defined at energies comparable to the bandwidth  $\Lambda$ . In pnictides, this scale is  $2 - 3eV$ , much larger than the Fermi energy  $E_F \sim 0.1eV$ . SC and SDW instabilities likely come from even smaller energies because instability temperatures are at least order of magnitude smaller than  $E_F$ . The couplings vary as one integrates out higher energies. This variation (i.e., the flow of the couplings from  $\Lambda$  down to the running scale  $E$ ) can be generally captured by the RG technique. In pnictides, the flow is different above and below  $E_F$ . Above  $E_F$ , each of the couplings changes because of integrating out higher energy fermions in both particle-hole and particle-particle channels. The RG equations in this region are called parquet RG, because renormalizations extend in the two directions. Below  $E_F$ , each vertex continues to flow due to renormalizations in only one channel, either particle-hole or particle-particle, depending on the external momenta. The RG equations in this region are called ladder RG, because renormalizations extend only in one direction.

already within parquet RG. This situation is the most interesting one from physics perspective particularly because in several cases different vertices diverge simultaneously, and the fixed point has an enhanced symmetry (e.g., in the 2-band model, the vertices in SDW, SC, and orbital CDW channels all diverge at the fixed point which then has  $O(6)$  symmetry<sup>51,52</sup>). The instability at energies above  $E_F$  is, however, unlikely scenario for the pnictides because the largest instability temperature is only a fraction of  $E_F$ .

- The RG flow reaches  $E_F$  before couplings diverge (Fig. 2b). In this situation, parquet RG creates a hierarchy of the couplings at  $E_F$ :  $\Gamma_i(E_F)$ . Below  $E_F$ , different  $\Gamma_i$  decouple and, for a perfect nesting, each continues evolving according to a ladder RG, i.e., like  $\Gamma_i(E) = \Gamma_i(E_F)/(1 - \Gamma_i(E_F) \log \frac{E_F}{E})$ . The instability occurs at the energy (temperature) at which  $\Gamma_i(E_F) \log \frac{E_F}{E} = 1$ . Obviously, the winning channel is the one in which the coupling is the largest at  $E_F$ .
- When nesting is not perfect (i.e., energies of the top of the hole band and of the bottom of the electron band are not exactly opposite), the coupling in the SC channel continues to follow  $\Gamma^{SC}(E) = \Gamma^{SC}(E_F)/(1 - \Gamma^{SC}(E_F) \log \frac{E_F}{E})$  simply because SC instability involves pairs of fermions with  $\mathbf{k}$  and  $-\mathbf{k}$  from the same FS and is non-sensitive to a devia-

tion from perfect nesting. However the logarithmic flow of SDW and CDW vertices is now cut at some scale  $E_b$ . Suppose  $E_b < E_F$  (Fig. 2c). In this situation, SC eventually wins over SDW and CDW instabilities, even if superconducting  $\Gamma$  is subleading at  $E_F$  (but it needs to be attractive at  $E_F$ ).

- When  $E_b$  exceeds  $E_F$  (Fig. 2d) particle-hole and particle-particle channels decouple already within the applicability range of parquet RG. At  $E < E_b$ , SC vertex continues to grow as  $\Gamma^{SC}(E) = \Gamma^{SC}(E_b)/(1 - \Gamma^{SC}(E_b) \log E_b/E)$ , while vertices in density-wave channels get frozen at their values at  $E \sim E_b$ . In this situation, SC instability again wins, even if it was subleading at  $E_b$ , provided that the superconducting vertex is attractive at  $E_b$ .

A subtle point: below we will be presenting the RG flows of vertices and couplings at energies both above and below  $E_F$  in terms of the logarithmic variable  $L \sim \log E$ . One has to bear in mind, however, that the prefactor for the logarithm actually changes between  $E > E_F$  and  $E < E_F$  because for  $E > E_F$  the integration over intermediate energies involves only positive excitations for electron states (and negative for hole state), i.e.,  $\int \frac{d^2k}{(2\pi)^2} = (m/2\pi) \int_E^\Lambda d\epsilon_k$ , while for  $E < E_F$ , one has to linearize the dispersions of holes and electrons near the FS and integrate on both sides of  $E_F$ , i.e.,  $\int \frac{d^2k}{(2\pi)^2} = (m/\pi) \int_E^{E_F} d\epsilon_k$ . To simplify the presentation we just define

$$L = \begin{cases} \frac{1}{2} \ln \frac{\Lambda}{E} & , E > E_F \\ \frac{1}{2} \ln \frac{\Lambda}{E_F} + \ln \frac{E_F}{E} & , E < E_F \end{cases}$$

and use the same symbol  $L$  for all energies. This is valid as long as we describe the system behavior at  $E \gg E_F$  and  $E \ll E_F$ . The behavior in the crossover regime  $E \sim E_F$  is more complex, but this is beyond the scope of the present paper. We will also use  $L_{E_F} \equiv \frac{1}{2} \ln \frac{\Lambda}{E_F}$ .

## B. Incorporating angular dependence

As we said in the Introduction, multi-orbital character of low-energy excitations in Fe-pnictides implies that interactions between fermions located near hole or electron FSs depend on the angles along the FSs. To obtain angular dependence of various couplings from first principles, one has to transform from five-orbital to five-band picture and dress up Coulomb interactions by coherence factors. This has been done in several studies (see, e.g., Refs. 24,26,53), under the assumption that the Coulomb interaction is so strongly screened that it can be replaced by Hubbard  $U$ . This assumption is generally valid for systems with large FSs, because of many available particle-hole pairs for screening, but in systems with small FSs, like pnictides, much fewer number of particle-hole pairs are available, and the screening of Coulomb interaction

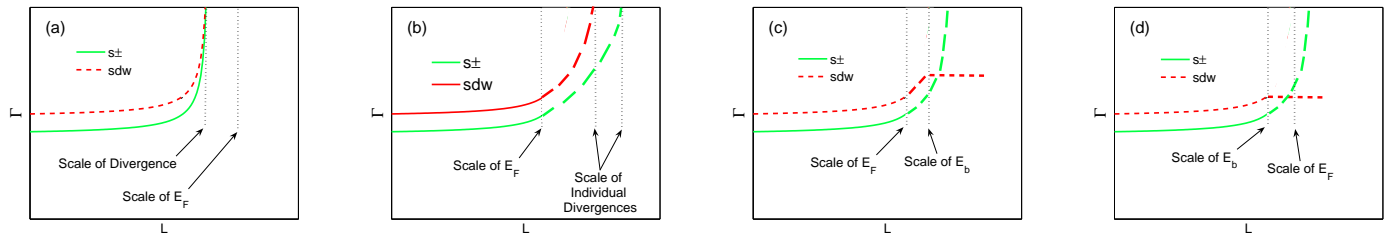


FIG. 2: Schematics of the RG flow of SC and SDW vertices  $\Gamma^{SDW}$  and  $\Gamma^{s\pm}$ . The horizontal scale is  $L = \frac{1}{2}\ln\frac{\Lambda}{E}$  for  $E > E_F$  and  $\frac{1}{2}\ln\frac{\Lambda}{E_F} + \ln\frac{E_F}{E}$  for  $E < E_F$ . SC and SDW vertices remain coupled at energies larger than  $E_F$  but decouple below  $E_F$ . Depending on the bare values of the vertices, the ratio  $\Lambda/E_F$ , and the doping, four different scenarios are possible (panels (a)-(d)). For perfect nesting, there are two possibilities: (a) the vertices diverge at the same scale before the scale of  $E_F$  is reached. The ratio of the vertices not necessarily tends to one, though. (b)  $E_F$  is reached before the vertices diverge. Then, below  $E_F$ , the vertices decouple, flow and diverge independently, each on its own scale. The vertex that had larger value at  $E_F$  diverges first and sets the instability. For non-perfect nesting (e.g., at a finite doping), SDW vertex eventually does not diverge. SC vertex still diverges, and the system becomes a SC even if SC instability was subleading at perfect nesting. The flow of the SDW vertex levels off either at  $E_b < E_F$  (panel c), or at  $E_b > E_F$  (panel d).

is much weaker, and is actually a rather non-trivial phenomenon at small  $k_F$ <sup>54</sup> Because of this complication, the “first-principle” analysis of the angular dependence of the interaction is a rather difficult task.

One can, however, attempt to extract these angular dependence from symmetry considerations, like it has been done for the cuprates<sup>55</sup> This is what we will do. Consider first the pairing vertex between fermions with incoming momenta  $k$  and  $-k$  and outgoing momenta  $p$  and  $-p$ . Quite generally, for tetragonal  $D_{4h}$  symmetry group, this interaction can be divided into one- and two-dimensional representation, and one-dimensional representation can be further divided into  $A_{1g}$ ,  $B_{1g}$ ,  $B_{2g}$ , and  $A_{2g}$  harmonics, depending on the symmetry under the transformations under  $k_{x,y} \rightarrow -k_{x,y}$  and  $k_x \rightarrow k_y$ . Basic functions from different representations do not mix, but each contains infinite number of components.  $s$ -wave pairing corresponds to fully symmetric  $A_{1g}$  representation. The  $s$ -wave pairing interaction can be quite generally expressed as

$$u(k, p) = \sum_{m,n} A_{mn} \Psi_m(k) \Psi_n(p) \quad (2)$$

where  $\Psi_m(k)$  are the basis functions of the  $A_{1g}$  symmetry group: 1,  $\cos k_x \cos k_y$ ,  $\cos k_x + \cos k_y$ , etc, and  $A_{mn}$  are coefficients. Suppose for definiteness that  $k$  belongs to hole FS and is close to  $k = 0$ . Expanding *any* wave function with  $A_{1g}$  symmetry near  $k = 0$ , one obtains along  $|\mathbf{k}| = k_F$ ,

$$\Psi_m(k) = a_m + b_m \cos 4\phi_k + c_m \cos 8\phi_k + \dots \quad (3)$$

If  $\mathbf{p}$  is near the same hole FS, the expansion of  $\Psi_n(p)$  also involves  $\cos 4\phi_p$ ,  $\cos 8\phi_p$ , etc. There are no fundamental reasons to expect that  $b_m$ ,  $c_m$ , etc are much smaller than  $a_m$ , but sub-leading terms are often small numerically. Two known examples are the

numerical smallness of  $\cos 6\phi$ , etc components of the  $d_{x^2-y^2}$ -wave gap for spin-fluctuation mediated pairing in the cuprates<sup>56</sup> and the numerical smallness of  $\cos 4\phi$ , etc components of the gap along the hole FSs in fRG<sup>27</sup> and RPA<sup>24,61</sup> calculations for 5-band Hubbard-type model for the pnictides. Taking these examples as circumstantial evidence, we assume that  $\cos 4\phi$ , etc terms are small. If so, the interaction between fermions belonging to the hole FS can be approximated by angle-independent term.

The situation changes, however, when we consider pairing interaction between fermions belonging to different FSs. Suppose that  $k$  are still near the center of the Brillouin zone, but  $p$  are near one of the electron FSs, say the one centered at  $(0, \pi)$ . Consider all possible  $\Psi_n(p)$  with  $A_{1g}$  symmetry. A simple experimentation with trigonometry shows that there are two different subsets of basic functions:

$$\begin{aligned} A : & 1, \cos p_x \cos p_y, \cos 2p_x + \cos 2p_y, \dots \\ \bar{A} : & \cos p_x + \cos p_y, \cos 3p_x + \cos 3p_y, \dots \end{aligned} \quad (4)$$

Functions from class A have the same properties as before – they can be expanded in series of  $\cos 4l\phi_p$  ( $l$  is integer). Functions from class  $\bar{A}$  are different – they all vanish at  $(0, \pi)$  and are expanded in series of  $\cos(2\phi_p + 4l\phi_p)$  (i.e., the first term is  $\cos 2\phi_p$ , the second is  $\cos 6\phi_p$ , etc). Let’s make the same approximation as before and neglect all terms with  $l > 0$ . The functions from class A can then be approximated by a constant, but the functions from class  $\bar{A}$  are approximated by  $\cos 2\phi_p$ . As a result,  $s$ -wave pairing interaction involving fermions from hole and one of the two electron FSs (labeled as  $e_1$ ) has a generic form of

$$\begin{aligned} u_{e_1,h}(k, p) &= u_{e_1,h} + \bar{u}_{e_1,h} \cos 2\phi_{p_{e_1}} + \dots \\ &= u_{e_1,h} (1 + 2\alpha \cos 2\phi_{p_{e_1}}) + \dots \end{aligned} \quad (5)$$

where dots stand for  $\cos 4\phi_k, \cos 4\phi_p, \cos 6\phi_p$ , etc terms. We emphasize that the constant term and the  $\cos 2\phi_p$  term in (5) are the leading terms of the two subsets of interaction terms, each form series in  $\cos 4\phi_{k,p}$ . By the same reasoning, the interaction between fermions near two electron FSs centered at  $(0, \pi)$  and  $(\pi, 0)$  is expressed as

$$u_{e_1, e_2}(k, p) \sim u_{e_1, e_2} (1 + 2\alpha' (\cos 2\phi_{k_{e_1}} + \cos 2\phi_{p_{e_2}}) + 4\alpha'' \cos 2\phi_{k_{e_1}} \cos 2\phi_{p_{e_2}} + \dots) \quad (6)$$

Observe also that the  $\cos 2\phi$  terms in (5) and (6) change sign under the transformation  $x \rightarrow y$  (like  $d_{x^2-y^2}$  interaction in the cuprates), hence the prefactor for  $\cos 2\phi_p$  term in (5) changes sign between the two electron FSs [ $\cos 2\phi_{p_{e_1}} \rightarrow -\cos 2\phi_{p_{e_2}}$ ].

The pairing interaction in the form of Eq. (5) has been introduced in Ref. 28. The authors of Ref. 28, however, didn't include into consideration the fact that band description is obtained from multi-orbital description and argued that  $\alpha$  must generally scale as  $k_F^2$  and should be small when  $k_F$  is small. In fact, the angular dependence produced by the coherent factors associated with the hybridization of 5  $Fe$  bands are not small in  $k_F$  (Refs. 24,53), hence  $\alpha, \alpha', \alpha''$  do not have to be small. Accordingly, we will keep  $\alpha$ 's as just parameters.

Once the pairing interaction has the form of Eqs. (5) and (6), the gap along hole FS is still angle-independent, but the gaps along the two electron FSs are in the form  $\Delta_e \pm \bar{\Delta}_e \cos 2\phi$ . When  $\bar{\Delta}_e$  is small compared to  $\Delta_e$ , the gaps on electron FSs are nearly angle-independent, but when  $|\bar{\Delta}_e| > |\Delta_e|$ , they have nodes at "accidental" values of  $\phi$ .

### C. The RG analysis with angle-dependent interactions

The angular dependence of the interaction is the key element of fRG approach, and this approach uses the full momentum dependence of the interactions, i.e., the full series of  $\cos 4l\phi$  and  $\cos(2\phi + 4l\phi)$  terms. At the same

time, fRG approach assumes renormalizability (i.e., that the right-hand side of each fRG equation contains only renormalized couplings, not some combinations of bare and renormalized couplings). In our analytical approach, we do calculations within logarithmic approximation in which case we explicitly preserve renormalizability.

We found, after explicitly evaluating the renormalizations of angle-dependent vertices, that the only way to justify RG procedure in this situation is to keep the angular dependence away from RG flow, i.e. allow  $u_{e_1, e_2}, u_{e_1, h}$ , and  $u_{e_2, h}$  to flow under RG, while  $\alpha, \alpha'$  and  $\alpha''$  are kept unchanged. This can be rigorously justified when  $\alpha$ 's are small and all terms of order  $\alpha^2$  are neglected. We will assume without proof that the results of RG analysis are valid even when  $\alpha \leq 1$ . There are no new physical effects at  $\alpha \leq 1$  compared to  $\alpha \ll 1$ , so the results at  $\alpha \leq 1$  should be at least qualitatively correct by continuity.

As we said in the Introduction, the main goal of our analysis is to understand whether there are qualitative differences between RG flow and the pairing in 2, 4, and 5 pocket models for  $Fe$ -pnictides. The next three sections deal with the comparison of 2,4, and 5-pocket models.

## III. THE 2 POCKET MODEL

This has been studied before ( Refs. 22,51) and we briefly review it here to set notations and for further comparisons with multi-pocket cases.

The 2 pocket model is a toy model consisting of one hole pocket in the center the folded Brillouin Zone (BZ), and four electron pockets at the corners as shown in Fig 3. To obtain parquet RG equations, we consider energies larger than  $E_F$  and  $E_b$ . At such energies deviations from perfect nesting become irrelevant, and we can set  $E_F, E_b \rightarrow 0$  and take hole and electron dispersions to be just opposite in sign.

The interaction Hamiltonian for the 2-pocket model is (following earlier notations<sup>22</sup>)

$$\begin{aligned} \frac{m}{2\pi} H_{int} = & \sum u_1 c_{p_1 s}^\dagger f_{p_2 s'}^\dagger f_{p_4 s'} c_{p_3 s} + \sum u_2 c_{p_1 s}^\dagger f_{p_2 s'}^\dagger c_{p_4 s'} f_{p_3 s} + \sum \frac{u_3}{2} \left( c_{p_1 s}^\dagger c_{p_2 s'}^\dagger f_{p_4 s'} f_{p_3 s} + h.c. \right) \\ & + \sum \frac{u_4}{2} f_{p_1 s}^\dagger f_{p_2 s'}^\dagger f_{p_4 s'} f_{p_3 s} + \sum \frac{u_5}{2} c_{p_1 s}^\dagger c_{p_2 s'}^\dagger c_{p_4 s'} c_{p_3 s} \end{aligned} \quad (7)$$

where  $u_i$  are dimensionless couplings, and  $m$  is quasiparticle mass ( $\varepsilon_f(k) = k^2/2m - \mu$ ). The sum is over the spin indices  $s$  and  $s'$  and the vector momenta  $p_1, p_2, p_3, p_4$  with momentum conservation assumed. The  $c$  and  $f$  fermions reside at the hole and the electron bands respectively. We

remind the reader that there is no angular dependence of the interactions here because the first angular term that comes in is  $\cos 4\phi$  which we ignore in our approximation.

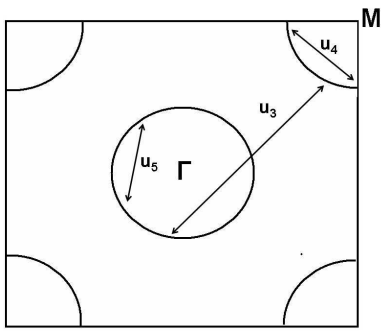


FIG. 3: Hole (center) and electron (corners) FSs in the folded BZ for 2-pocket model. The arrows with symbols indicate intra-pocket and inter-pocket pairing interactions ( $u_4$  and  $u_5$  are intra-pocket interactions, and  $u_3$  is inter-pocket interaction). There also exist density-density and exchange interactions between hole and electron pockets ( $u_1$  and  $u_2$  terms, respectively, not shown).

### A. The Vertices

We begin by looking into the vertices in SC and SDW channels. For this, we introduce infinitesimally small SC and SDW order parameters  $\Delta_{SC}^o$  and  $\Delta_{SDW}^o$ , dress them up by including multiple interactions as shown diagrammatically in Fig. 4, and write the renormalized order parameters in the form

$$\Delta_i = \Delta_i^o (1 + \Gamma_i L) \quad (8)$$

where  $\Gamma_i$  satisfies  $\frac{d\Gamma_i}{dL} = \Gamma_i^2$

For a given  $i$ ,  $\Delta_i$  becomes nonzero even for vanishing  $\Delta_i^o$  when the corresponding  $\Gamma_i$  diverges.

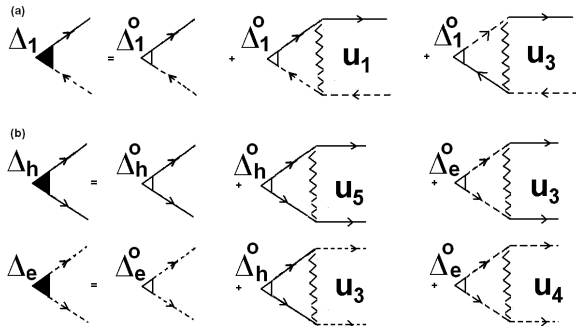


FIG. 4: Diagrams for the renormalization of infinitesimally small SDW and SC vertices, added to the Hamiltonian in order to calculate response functions. Unshaded triangles - bare vertices, shaded triangles - full vertices, wave lines - fully renormalized interactions. Solid lines correspond to  $c$  fermions and the dashed line to  $f$  fermions.  $\Delta_1$  is SDW vertex and  $\Delta_h$  and  $\Delta_e$  are SC vertices on hole and electron FSs.

The computations for the 2-pocket model is straightforward. For the SDW order parameter, we immediately

obtain from Fig. 4,  $\Gamma^{SDW} = u_1 + u_3$ . For the SC channel, we obtain from Fig. 4

$$\begin{pmatrix} 1 - u_5 L & -u_3 L \\ -u_3 L & 1 - u_4 L \end{pmatrix} \begin{pmatrix} \Delta_h^o \\ \Delta_e^o \end{pmatrix} = \begin{pmatrix} \Delta_h \\ \Delta_e \end{pmatrix} \quad (9)$$

where  $\Delta_{e,h}$  are order parameters on hole and electron FSs. Diagonalizing this set and casting the result in the form of Eq. (8), we obtain two SC  $\Gamma$ 's. One corresponds to a conventional  $s$ -wave pairing, is repulsive for all positive  $u_i$  and is of no interest to us, another corresponds to  $s \pm$  pairing and is given by

$$\Gamma^{s\pm} = \frac{-(u_4 + u_5) + \sqrt{(u_4 - u_5)^2 + 4u_3^2}}{2} \quad (10)$$

For  $u_4 = u_5$ ,  $\Gamma^{s\pm}$  reduces to  $\Gamma^{s\pm} = -u_4 + u_3$ .

The SDW vertex is attractive for positive  $u_1$  and  $u_3$ , while  $\Gamma^{s\pm}$  is attractive only when inter-band pair hopping term exceeds intra-band repulsive interaction. Like we said, this is very unlikely because both interactions originate from Coulomb interaction, and screened Coulomb interaction at small momentum transfer (i.e.,  $u_4$  and  $u_5$ ) is larger than that at large momentum transfer (i.e.,  $u_3$ ).

To understand whether the negative sign of  $\Gamma^{s\pm}$  can be reversed, we need to consider RG flow of the couplings. This what we do next.

### B. RG flow between $\Lambda$ and $E_F$

The RG equations for the couplings have been obtained in<sup>22</sup>, and we just quote the result:

$$\begin{aligned} \dot{u}_4 &= -[u_4^2 + u_3^2] \\ \dot{u}_5 &= -[u_5^2 + u_3^2] \\ \dot{u}_1 &= [u_1^2 + u_3^2] \\ \dot{u}_2 &= [2u_1 u_2 - 2u_2^2] \\ \dot{u}_3 &= [4u_1 u_3 - 2u_2 u_3 - (u_4 + u_5)u_3] \end{aligned} \quad (11)$$

The derivatives are with respect to  $L$ . These equations have a single non-trivial fixed point at which all couplings diverge and tend to  $u_3 = \sqrt{5}u_1$ ,  $u_4 = u_5 = -u_1$ ,  $u_2 \propto (u_1)^{1/3}$ . The flow of SDW and SC vertices is shown in Fig. 6a. In the process of RG flow, the SC vertex  $\Gamma^{s\pm}$  changes sign and become attractive. The ratio  $\Gamma^{s\pm}/\Gamma^{SDW}$  remains smaller than one during the flow, but tends to one upon approaching the fixed point, i.e., if this fixed point is reached within parquet RG, superconducting and SDW instabilities occur simultaneously, and the system actually cannot distinguish between the two. There is another vertex which tends to the same value as SDW and SC vertices - it corresponds to an CDW instability with imaginary order parameter (an instability towards orbital currents), The combination of 3-component SDW, 2-component SC and 1-component



CDW instabilities makes the fixed point  $O(6)$  symmetric<sup>52</sup>.

The sign change of the superconducting  $\Gamma^{s\pm}$  is the most notable effect within the parquet RG flow. Its physics originates in the effective ‘‘attraction’’ between SC and SDW fluctuations (not the order parameters!), namely from the fact that  $u_3$ , which is the attractive component of  $\Gamma^{s\pm}$ , gets the boost from  $u_1$ , which contributes to  $\Gamma^{SDW}$ . The boost is  $4u_1u_3$  term in the r.h.s. of the RG equation for  $\dot{u}_3$ . This term overshadows the negative effect from  $u_2$ ,  $u_4$ , and  $u_5$ , and as a result  $u_3$  increases under RG. At the same time, intra-pocket repulsions  $u_4$  and  $u_5$  decrease under RG. At some point,  $u_3^2$  becomes larger compared to  $u_4u_5$ , and  $\Gamma^{s\pm}$  becomes positive.

However, as we said earlier, parquet RG is only valid at energies above  $E_F$ . It is unlikely that the fixed point is reached above  $E_F$ , otherwise there would be at least pseudogap effects present above  $E_F$ , but there is no strong evidence for pseudogap in the pnictides. More likely, the couplings evolve under parquet RG (and  $\Gamma^{s\pm}$  possibly changes sign at some scale), but  $u_i$  remain finite at  $E_F$ . To continue below this scale we need to derive a different set of equations, for which  $u_i(E_F)$  serve as initial conditions.

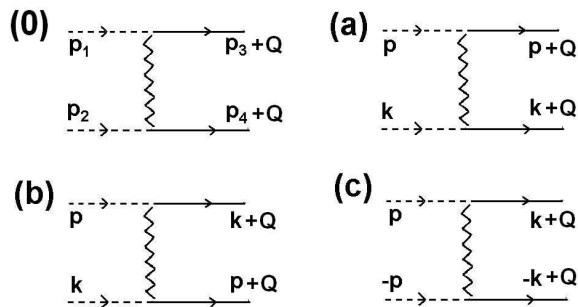


FIG. 5: (0) The  $u_3$  vertex with general momenta  $p_1, p_2, p_3+Q, p_4+Q$  (all  $p_i$  are small and  $p_1+p_2=p_3+p_4$ ). During calculations, three kinds of  $u_3$  vertices arise—(a) the one with  $p_1=p_3$ , (b) the one with  $p_2=p_3$ , and (c) the one with  $p_1+p_2=0$ . The vertex ‘b’ contributes to the renormalization in p-h channel, and the vertex ‘c’ contributes to the renormalization in the p-p channel.

### C. RG flow below the scale of $E_F$

The RG equations below  $E_F$  for 2-pocket model have been derived in Ref. 51 and we just quote the result. The most essential difference with the previous subsection concerns  $u_3$  vertex, which contributes to both SC and SDW channels. Below  $E_F$  the structure of the external momenta becomes relevant, and one has to distinguish between  $u_3^{(a)}$  with zero transferred momentum,  $u_3^{(b)}$  with momentum transfer  $Q$ , and  $u_3^{(c)}$  with zero total momentum (see Fig. Fig. 5). Each of the vertices

now undergoes logarithmic renormalization in its own channel, crossed renormalizations no longer contribute because internal  $E=O(E_F)$ , and the arguments of the corresponding logarithms become  $O(1)$ . The new equations are

$$\begin{aligned}\dot{u}_3^{(a)} &= 2u_1u_3^{(a)} - 2u_2u_3^{(a)} \\ \dot{u}_3^{(b)} &= 2u_1u_3^{(b)} \\ \dot{u}_3^{(c)} &= -[u_4 + u_5]u_3^{(c)} \\ \dot{u}_4 &= -[u_4^2 + (u_3^{(c)})^2] \\ \dot{u}_5 &= -[u_5^2 + (u_3^{(c)})^2] \\ \dot{u}_1 &= [u_1^2 + (u_3^{(b)})^2] \\ \dot{u}_2 &= [2u_1u_2 - 2u_2^2]\end{aligned}\quad (12)$$

where the derivatives are with respect to  $L$ . The effective vertices in the SDW and SC channels also get modified and become

$$\begin{aligned}\Gamma^{SDW} &= u_1 + u_3^{(b)} \\ \Gamma^\pm &= \frac{-(u_4 + u_5) + \sqrt{(u_4 - u_5)^2 + 4(u_3^{(c)})^2}}{2}\end{aligned}\quad (13)$$

One can easily verify that new vertices satisfy

$$\frac{d\Gamma_i}{dL} = \Gamma_i^2 \quad (14)$$

as it should be because SC and SDW channels are now decoupled (no cross-terms in RG equations).

The behavior of the vertices below  $E_F$  is illustrated in Fig. 6 b,c. If SC vertex is already positive (attractive) at  $E_F$  (Fig. 6b), it diverges at some scale below  $E_F$ , but for perfect nesting SDW vertex diverges first. Upon doping, SDW vertex levels off, and the first instability eventually becomes the SC one. If SC vertex remains negative at  $E_F$  (Fig. 6c), it decreases below  $E_F$  but still remains negative. In this situation,  $s^\pm$  SC does not appear even when SDW order gets killed by non-nesting.

To summarize: in a 2-pocket model three scenarios are possible: (i) the instability occurs simultaneously in SDW, SC, and CDW channels, and a fixed point has  $O(6)$  symmetry, (ii) SDW instability wins at perfect nesting, but yields to  $s^\pm$  superconductivity upon doping, and (iii) SDW instability exists near perfect nesting, but no SC instability emerges when SDW order is suppressed by doping. For the cases (i) and (ii), the SC gap has a simple plus-minus form, i.e., the gaps along hole and electron FSs are angle independent (up to  $\cos 4\phi$  terms which we neglected) and are of the opposite signs.

The 2-pocket model is indeed only a toy model for the pnictides. The actual band structure of the pnictides includes two electron FSs and at least two hole FSs. The question we now address is whether qualitatively new behavior emerges when we increase the number of pockets.

We argue below that there are new features not present in a 2-pocket model.

#### IV. 4 POCKET MODEL

We now consider the case of 2 hole and 2 electron FSs. We neglect  $k_z$  variation of the FSs and consider a cross section in XY plane. The two electron FSs are generally ellipses, centered at  $(0, \pi)$  and  $(\pi, 0)$  in the unfolded zone. The two hole FSs are circles centered at  $(0, 0)$ . They generally are of non-equal sizes, and one is less nested with electron FSs than the other.

The RG analysis of a generic 4-pocket model is straightforward but rather cumbersome. We show the results in the two more easily trackable limits: one when

the two hole FSs are completely equivalent, and the other when one of the two hole FSs is much weakly coupled with electron than the other one and can be neglected. In the second limit, 4-pocket model reduces to 3-pocket model<sup>28,57</sup>. We show that the system behavior is identical in the two limits, and make a conjecture that it doesn't evolve between the limits. We continue with our earlier assumption of circular electron FSs that nests with the hole FS.

We begin with the limit when one hole FS can be neglected and 4 pocket model reduces to 3 pocket model.

##### A. Effective model with one hole at $(0, 0)$ .

The interaction Hamiltonian for the 4-pocket model is

$$\begin{aligned}
\frac{m}{2\pi}H_{int} &= \sum u_1^{(1)} c_{p_1s}^\dagger f_{1p_2s'}^\dagger f_{1p_4s'} c_{p_3s} + \sum u_2^{(1)} c_{p_1s}^\dagger f_{1p_2s'}^\dagger c_{p_4s'} f_{1p_3s} + \sum \frac{u_3^{(1)}}{2} \left( c_{p_1s}^\dagger c_{p_2s'}^\dagger f_{1p_4s'} f_{1p_3s} + h.c. \right) \\
&+ f_1 \leftrightarrow f_2 \text{ and } u_i^{(1)} \leftrightarrow u_i^{(2)} \\
&+ \sum \frac{u_5}{2} c_{p_1s}^\dagger c_{p_2s'}^\dagger c_{p_4s'} c_{p_3s} + \sum \frac{u_4^{(1)}}{2} f_{1p_1s}^\dagger f_{1p_2s'}^\dagger f_{1p_4s'} f_{1p_3s} + \sum \frac{u_4^{(2)}}{2} f_{2p_1s}^\dagger f_{2p_2s'}^\dagger f_{2p_4s'} f_{2p_3s} \\
&+ \sum u_6 f_{1p_1s}^\dagger f_{2p_2s'}^\dagger f_{2p_4s'} f_{1p_3s} + \sum u_7 f_{1p_1s}^\dagger f_{2p_2s'}^\dagger f_{1p_4s'} f_{2p_3s} + \sum \frac{u_8}{2} \left( f_{1p_1s}^\dagger f_{1p_2s'}^\dagger f_{2p_4s'} f_{2p_3s} + h.c. \right)
\end{aligned} \tag{15}$$

This is a straightforward generalization of the 2-pocket case (see also Ref. 57). The notations are the same as for the 2-pocket model, but now  $f_1$  and  $f_2$  refer to fermions from the two different electron bands. The new terms  $u_6, u_7$ , and  $u_8$  are different inter-pocket interactions between  $f$ -fermions. Because we now have two different sets of electron state, it is convenient to work in the unfolded BZ, and in Fig 7 we show the interactions that contribute to the pairing vertex. There are, however, subtle effects related to the actual,  $As$ -induced differences between folded and unfolded zones, and we will discuss them below.

The two electron bands are related by symmetry  $k_x \leftrightarrow k_y$  (i.e.,  $\varepsilon_{f_1}(k_x, k_y) = \varepsilon_{f_2}(k_y, k_x)$ ), and it is natural to set  $u_i^{(1)} = u_x^{(i)} = u_i$  ( $i$  runs between 1 and 4). We verified that no new terms are generated under RG flow, however the interactions between electron pockets must be included as they anyway are generated by RG.

The angular dependence of the vertices is incorporated in the same manner as described in Sec. II, by including  $\alpha \cos 2\phi$  terms into the vertices which involve fermions near electron pockets. To simplify calculations, we first neglect the angular dependence of the intrapocket electron-electron interaction  $u_4$ . Later we show that including angular dependence of  $u_4$  will not change the results qualitatively.

##### 1. The Vertices

The computational procedure is the same as before. We introduce infinitesimally small SC and SDW vertices, dress them up by the interactions, and express the renormalized vertices in terms of the running couplings.

The diagrammatic expressions for the renormalized vertices are presented in Fig. 8. For the SDW vertex we have  $\Delta^{SDW} = \Delta_1^{SDW} + \Delta_2^{SDW} \cos 2\phi$ ,  $\phi$  being the angle along the electron FS. For SC vertex on the hole FS  $\Delta^{SC} = \Delta_h$  and on the two electron FSs  $\Delta^{SC} = \Delta_e \pm \tilde{\Delta}_e \cos 2\phi$ , as required by symmetry for an  $s$ -wave gap. If  $|\tilde{\Delta}_e| > |\Delta_e|$ , the SC gap has nodes along the FS. The nodes are ‘accidental’ in the sense that they are not protected by any symmetry.

For the SC vertex we then obtain the coupled set of equations

$$\begin{pmatrix} 1 - u_5L & -2u_3L & -2\alpha u_3L \\ -u_3L & 1 - \tilde{u}_4L & 0 \\ -2\alpha u_3L & 0 & 1 \end{pmatrix} \begin{pmatrix} \Delta_h^o \\ \Delta_e^o \\ \tilde{\Delta}_e^o \end{pmatrix} = \begin{pmatrix} \Delta_h \\ \Delta_e \\ \tilde{\Delta}_e \end{pmatrix} \tag{16}$$

where  $\tilde{u}_4 = u_4 + u_8$ . For the SDW vertex we obtain (assuming that  $\Delta_{1,2}$  are real)

$$\begin{pmatrix} 1 + (u_1 + u_3)L & \frac{\alpha}{2}(u_1 + u_3)L \\ \alpha(u_1 + u_3)L & 1 \end{pmatrix} \begin{pmatrix} \Delta_1^o \\ \Delta_2^o \end{pmatrix} = \begin{pmatrix} \Delta_1 \\ \Delta_2 \end{pmatrix} \tag{17}$$

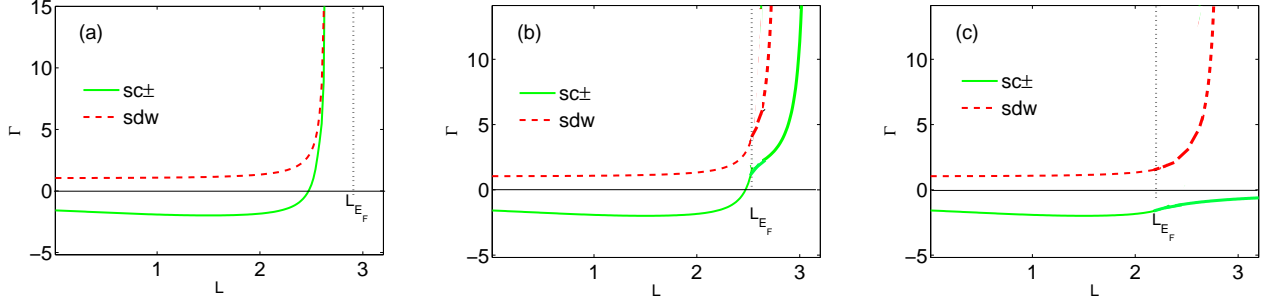


FIG. 6: Running vertices in SDW and SC  $s\pm$  channel for the 2-pocket case at perfect nesting as functions of  $L$ . Three qualitatively different scenario are possible: (a) vertices diverge before  $L_{E_F}$  is reached. Both vertices flow to the same fixed point, their ratio tends to one, and the fixed point has an extended symmetry. (b)  $L_{E_F}$  is reached before the fixed point, but in the range of  $L$  where the SC vertex is already attractive (positive). The vertices flow independent of each other beyond  $L_{E_F}$  (below  $E_F$ ), the SDW vertex diverges first. On doping SDW yields to SC (see Fig. 2). (c) The value  $L_{E_F}$  is reached when SC vertex is still repulsive (negative). In this case SC instability does not occur even after SDW instability is eliminated by doping.

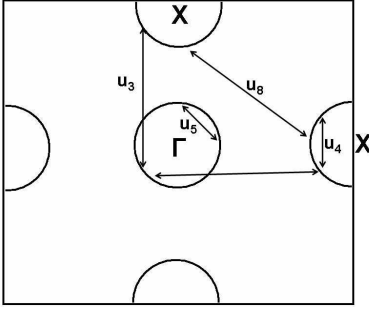


FIG. 7: Hole (center) and electron(edges) FSs in the unfolded BZ for 4-pocket model. The arrows with symbols indicate various intra-pocket and inter-pocket interactions which contribute to the SC vertex. There exist other density-density and exchange inter-pocket interactions ( $u_1$ ,  $u_2$ ,  $u_6$ , and  $u_7$  terms, not shown).

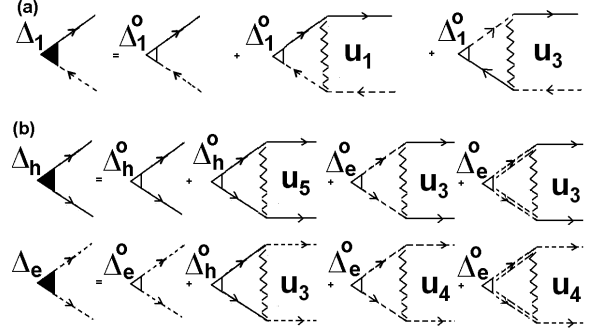


FIG. 8: The diagrams for the SDW and SC vertices for the 4-pocket model (panels (a) and (b)). The notations are the same as in Fig.4. Single and double dashed lines describe fermions from the two electron bands.

We included angular dependence of both  $u_3$  and  $u_1$  terms and for simplicity set  $\alpha$  to be the same for both. Observe that  $\alpha$ -dependent terms appear in SDW vertex with extra  $1/2$  compared to SC vertex. This is because internal and external part of the SDW vertex each contains one fermion from the electron FS, while in the SC vertex there are two such fermions, either in the internal or in the external part. One can easily check that in the SC vertex all  $\alpha$ -terms then appear with extra factor of 2 compared to SDW vertex.

The effective vertices are found by diagonalizing these matrices and casting the results into the forms  $\Delta_i = \Delta_i^o(1 + \Gamma_i L)$ . For  $\alpha = 0$ , the formulas simplify and we have

$$\begin{aligned} \Gamma_1^{SC} = \Gamma^{s\pm} &= \frac{-(\tilde{u}_4 + u_5) + \sqrt{(\tilde{u}_4 - u_5)^2 + 8(u_3)^2}}{2} \\ \Gamma_2^{SC} = \Gamma^{s++} &= \frac{-(\tilde{u}_4 + u_5) - \sqrt{(\tilde{u}_4 - u_5)^2 + 8(u_3)^2}}{2} \\ \Gamma^{SDW} = \Gamma_1^{SDW} &= u_1 + u_3 \end{aligned} \quad (18)$$

The solutions corresponding to  $\Gamma_1$  and  $\Gamma_2$  are  $\Delta_h/\Delta_e < 0$  and  $\Delta_h/\Delta_e > 0$ , accordingly, hence the notations  $\Gamma^{s\pm}$  and  $\Gamma^{s++}$ . The vertex  $\Gamma^{s++}$  is repulsive for all couplings, while  $\Gamma^{s\pm}$  is repulsive for  $2u_3^2 < \tilde{u}_4 u_5$  and is attractive for  $2u_3^2 > \tilde{u}_4 u_5$ . The SDW vertex is attractive. We recall that  $u_4$  and  $u_5$  are Coulomb interactions at small momentum transfer, while  $u_3$  and  $u_8$  are Coulomb interactions at large momentum transfer and are supposed to be smaller than  $u_5$ ,  $u_4$ . At the bare level then there is no attractive component of  $\Gamma^{SC}$  for  $\alpha = 0$ .

At a finite  $\alpha$  we obtain two SDW vertices  $\Gamma_1^{SDW} = (u_1 + u_3)(1 + \sqrt{1 + 2\alpha^2})/2$  and  $\Gamma_2^{SDW} = -(u_1 + u_3)(\sqrt{1 + 2\alpha^2} - 1)/2$ . The second one is repulsive, which

the first one is attractive and only increases with  $\alpha$ . For the SC vertex, the three  $\Gamma_i^{SC}$  are obtained by diagonalizing Eq. (16) what requires solving the cubic equation. The analytical expressions for  $\Gamma_i^{SC}$  are long and we refrain from presenting them (we will show all three  $\Gamma_i^{SC}$  in the figures). It is essential, however, that for *any*  $\alpha \neq 0$ , one of three  $\Gamma_i^{SC}$  is attractive even when  $\tilde{u}_4 u_5$  is larger than  $2u_3^2$  and at  $\alpha = 0$  SC vertices are repulsive. At small  $\alpha$ , we have for such induced solution

$$\Gamma_1^{SC} = \alpha^2 \left[ \frac{4u_3^2 u_5}{\tilde{u}_4 u_5 - 2u_3^2} \right], \quad \tilde{u}_4 u_5 > 2u_3^2 \quad (19)$$

Other two solutions  $\Gamma_{2,3}^{SC}$  are negative, i.e. repulsive.

For  $\tilde{u}_4 u_5 < 2u_3^2$ , the attractive solution exists already at  $\alpha = 0$ , and is only weakly affected by  $\alpha$ . For  $\tilde{u}_4 u_5 < 2u_3^2$  we have:

$$\Gamma_1^{SC} = \Gamma^{s\pm} \left[ 1 + \alpha^2 \left( \frac{2u_3^2 (-\Delta u + \sqrt{(\Delta u)^2 + 8u_3^2})}{(\Gamma^{s\pm})^2 \sqrt{(\Delta u)^2 + 8u_3^2}} \right) \right] \quad (20)$$

where  $\Delta u = \tilde{u}_4 - u_5$  and  $\Gamma^{s\pm}$  is given by Eq. 18. The other two  $\Gamma_{2,3}^{SC}$  are again negative.

We now proceed with the RG flow.

## 2. RG flow between $\Lambda$ and $E_F$

Like in 2-pocket case, at  $\Lambda > E > E_F$ , renormalizations in p-h and p-p channels are logarithmical and independent of the location of external momenta. The derivation of parquet RG equations is straightforward but requires more efforts as there are new terms in the Hamiltonian. For illustration, we show in Fig 9 the diagrams contributing to the renormalization of the vertices  $u_4$  and  $u_3$ . The diagrams for the renormalization of other vertices are similar.

Collecting the diagrams for the renormalization of all couplings, we find that the terms  $u_6 \pm u_7$  and  $u_4 - u_8$  are decoupled from the rest of the terms and are renormalized as  $\dot{u}_j = -(u_j)^2$ . Because all these  $u_j$  are the differences between Coulomb interactions at small and large momentum transfers, their bare values are positive in which case the these interactions flow to zero under RG and are therefore irrelevant.

The other five vertices are all coupled and flow according to

$$\begin{aligned} \dot{u}_5 &= -[u_5^2 + 2u_3^2] \\ \dot{\tilde{u}}_4 &= -[\tilde{u}_4^2 + 2u_3^2] \\ \dot{u}_1 &= +[u_1^2 + u_3^2] \\ \dot{u}_2 &= +[2u_1 u_2 - 2u_3^2] \\ \dot{u}_3 &= +[4u_1 u_3 - 2u_2 u_3 - u_5 u_3 - \tilde{u}_4 u_3] \end{aligned} \quad (21)$$

This set of equations can be easily solved numerically. Fig 10 shows the plot of  $u_5/u_1$ ,  $\tilde{u}_4/u_1$ ,  $u_2/u_1$ , and  $u_3/u_1$

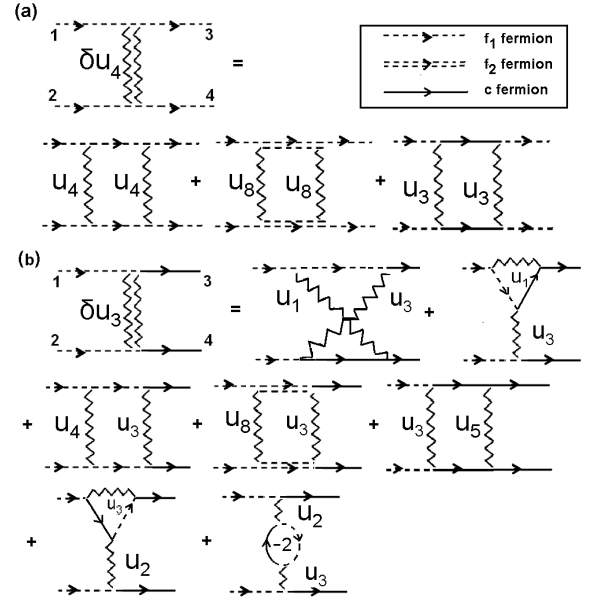


FIG. 9: Second order diagrams for the renormalizations of  $u_4$  and  $u_3$  vertices (panels a and b, respectively). The combinatorial factors are not shown but must indeed be included.

with  $L$ . For simplicity, we set bare values of  $\tilde{u}_4$  and  $u_5$  to be equal – the two then remain equal in the process of RG flow. The values of the ratios at the fixed point are indicated by the dots. These can be easily found analytically by requesting that all 5 equations in (21) be identical. Imposing this condition we obtain  $u_5/u_1 = \tilde{u}_4/u_1 = -\sqrt{6} \approx -2.45$ ,  $u_3/u_1 = (3 + 2\sqrt{6})^{1/2} \approx 2.81$ ,  $u_2/u_1 = 0$ . Like in 2-pocket model, intra-pocket repulsions  $\tilde{u}_4$  and  $u_5$  decrease under RG, change sign at some value of  $L$ , and become negative at larger  $L$ . This sign change (overscreening) goes beyond a conventional McMillan-Tolmachev screening of the Coulomb interaction, and is the result of the “push” from  $u_3$ , which in turn increases under RG due to the “push” from  $u_1$  which contributes to the SDW vertex. So, eventually, overscreening is the result of the “attraction” between SDW and SC fluctuations. The difference  $\tilde{u}_4 u_5 - 2u_3^2$  also changes sign at some  $L$  and becomes negative at larger  $L$ .

We now substitute the running couplings into the expressions for SC and SDW vertices and check how they flow. The results are presented in Fig. 11 for  $\alpha = 0.4$ . For the SDW vertices, the positive one increases with  $L$ , like in the 2-pocket model, while the negative one becomes more negative, i.e., even less relevant. For the SC vertices,  $\Gamma_1^{SC}$  is positive for all  $L$ , the other two  $\Gamma_{2,3}^{SC}$  are negative and hence irrelevant. The positive  $\Gamma_1^{SC}$  interpolates between Eq. (19) at small  $L$ , and Eq. (20) at larger  $L$ . We emphasize that for all values of  $L$  this is the same solution, i.e., there is no level crossing (see Fig. 11).

In Fig. 12a we compare the behavior of  $\Gamma^{SDW}$  and  $\Gamma^{SC}$  as functions of  $L$  assuming that the fixed point is reached at energies above  $E_F$ . At small  $L$ , we have the same situation as in 2-pocket model: SDW vertex is larger than

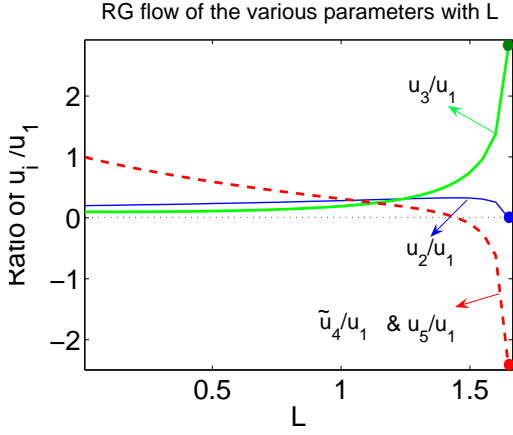


FIG. 10: The solution of Eq. (21) – the RG flow of  $u_5$ ,  $\tilde{u}_4$ ,  $u_2$ , and  $u_3$  (all relative to  $u_1$ ) with  $L$ . For simplicity, we set bare values of  $\tilde{u}_4$  and  $u_5$  equal. Note how, as fixed point is approached, the renormalized Coulomb repulsion at small momenta ( $u_5$  and  $\tilde{u}_4$  terms) is suppressed and eventually changes sign, while the pair hopping term  $u_3$  is strengthened.

SC vertex. However, the rate of increase of the SC vertex exceeds that of the SDW vertex, and at some  $L$  before the fixed point is reached,  $\Gamma^{SC}$  crosses over  $\Gamma^{SDW}$  implying that superconductivity becomes the leading instability even at perfect nesting. Such crossing has been reported in fRG calculations<sup>27</sup> for the same model. We view the agreement as a good indication that numerical fRG and analytical parquet RG approaches describe the same physics. In our analytical RG, the reason for the crossing is combinatoric: compared to 2-pocket case (where SDW and SC vertices flow to the same value under RG), the presence of the second electron FS adds the factor of 2 to the renormalization of the SC vertex as a pair of fermions from the hole FS can hop to each of the two electron FSs. However, there is no such factor of 2 in the renormalization of the SDW vertex due to momentum conservation.

We emphasize that the crossing of  $\Gamma_1^{SDW}$  and  $\Gamma_1^{SC}$  is not related to the angular dependence of the interaction. Even when  $\alpha = 0$ , SC vertex exceeds SDW vertex near the fixed point of parquet RG. At the fixed point, the ratio of the two is  $\Gamma_1^{SC}/\Gamma_1^{SDW} \approx 1.69$ .

The SC order parameter by itself has an interesting character. We recall that we approximate the gap along the hole FS by a constant  $\Delta_h$  and approximate the gap along the two electron FSs by  $\Delta_e \pm \Delta_e \cos 2\phi$ . At small  $L$ , the attractive  $\Gamma^{SC}$  exists only because of a non-zero  $\alpha$ , and  $\bar{\Delta}_e$  is larger than  $\Delta_e$  (Ref. 28), hence the gap along the two electron FSs has “accidental” nodes. As  $L$  increases, the SC vertex  $\Gamma$  evolves, according to Fig. 11, and eventually gets close to the would-be solution for  $\alpha = 0$ . For the latter,  $\bar{\Delta}_e = 0$ , and the gap obviously has no nodes. The crossover from one limit to the other is displayed in Fig. 13, where we show the flow of the gaps  $\Delta_h$ ,  $\Delta_e$ , and  $\bar{\Delta}_e$ , corresponding to the leading SC

vertex. For the value of  $\alpha$  which we used in this figure ( $\alpha = 0.4$ ) the transition from nodal to nodeless gap occurs at  $L$  smaller than the one at which SC vertex crosses the SDW vertex, i.e., when SC becomes the leading instability, the superconducting gap is already nodeless. But for other values of  $\alpha$  we can get either nodeless or nodal SC in this regime. In Fig. 14 we plot the “phase diagram” coming out of parquet RG for different  $\alpha$  [the bare values of  $u_i$  are the same for all figures in this section]. In white region, SDW vertex is the largest and SC vertex is subleading, implying that superconductivity can be revealed only after SDW order is suppressed by doping. In the shaded region the SC vertex is the largest. We see that superconducting gap in this region can actually be either nodal or nodeless, depending on the value of  $\alpha$ . At  $\alpha = 0$ , the ratio of  $\Delta_e$  and  $\Delta_h$  at the fixed point is  $\Delta_h = -\sqrt{2}\Delta_e$ .

### 3. RG flow below the scale of $E_F$

We now consider the situation below  $E_F$ . As in the 2-pocket model, we have to introduce three different  $u_3$  couplings ( $u_3^{(a)}$ ,  $u_3^{(b)}$ , and  $u_3^{(c)}$ ) of which  $u_3^{(b)}$  is the part of SDW vertex, and  $u_3^{(c)}$  is the part of the SC vertex (the corresponding  $u_3^{(i)}$  replace  $u_3$  in Eqs. (16) and (17)). The flow of the couplings is now governed by

$$\begin{aligned}
 \dot{u}_5 &= - [u_5^2 + 2(u_3^{(c)})^2] \\
 \dot{\tilde{u}}_4 &= - [\tilde{u}_4^2 + 2(u_3^{(c)})^2] \\
 \dot{u}_1 &= + [u_1^2 + (u_3^{(b)})^2] \\
 \dot{u}_2 &= + [2u_1u_2 - 2u_2^2] \\
 \dot{u}_3^{(a)} &= 2u_1u_3^{(a)} - 2u_2u_3^{(a)} \\
 \dot{u}_3^{(b)} &= 2u_1u_3^{(b)} \\
 \dot{u}_3^{(c)} &= [u_5 + \tilde{u}_4]u_3^{(c)} \quad (22)
 \end{aligned}$$

Note the  $\tilde{u}_4$  and  $u_5$  have identical equations and hence treated identically. One can then straightforwardly verify using (22) that SC and SDW vertices decouple, as they should, and each satisfies  $\dot{\Gamma}_i = \Gamma_i^2$ . Hence, as before, whichever vertex is larger at  $E_F$  gives rise to the first instability as  $T$  decreases. If SC vertex prevails, the system becomes SC at perfect nesting and remains a SC at finite dopings (Fig. 12b). If SDW vertex prevails, the system becomes an SDW antiferromagnet at perfect nesting and then eventually becomes a SC upon doping (Fig. 12c). In distinction to the 2-pocket case, we don’t need to worry about the sign of the SC vertex once SDW instability is reduced by doping because one of  $\Gamma^{SC}$  is always attractive (see Fig. 11). We emphasize again that this attractive  $\Gamma^{SC}$  leads to either nodeless  $s\pm$  gap, or to  $s\pm$  gap with nodes along the electron FSs, depending

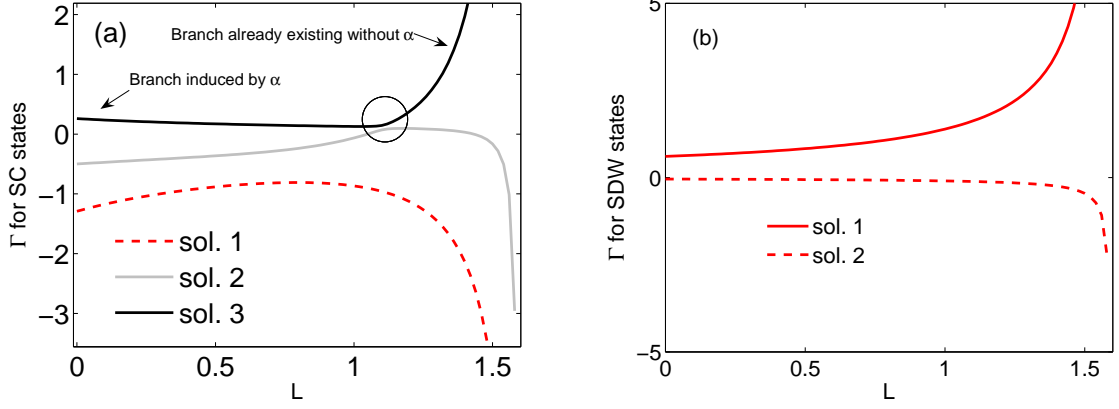


FIG. 11: The flow of SC and SDW vertices under RG in the effective 3-pocket model for  $\alpha = 0.4$ . Panel (a) 3 SC vertices. One solution is attractive for all  $L$  (and corresponds to  $s \pm$  pairing), the other two are repulsive. One of the repulsive solutions is of  $s \pm$  character, another of  $s ++$  character. At small  $L$ , the positive solution is the one induced by  $\alpha$ , at large  $L$  it almost coincides with the solution which becomes positive for these  $L$  already at  $\alpha = 0$ . The circle marks the area where positive and negative solutions come close to each other. The splitting between the two increases with  $\alpha$ . (b) The two SDW vertices. One vertex is always attractive (positive) and the other is repulsive (negative).

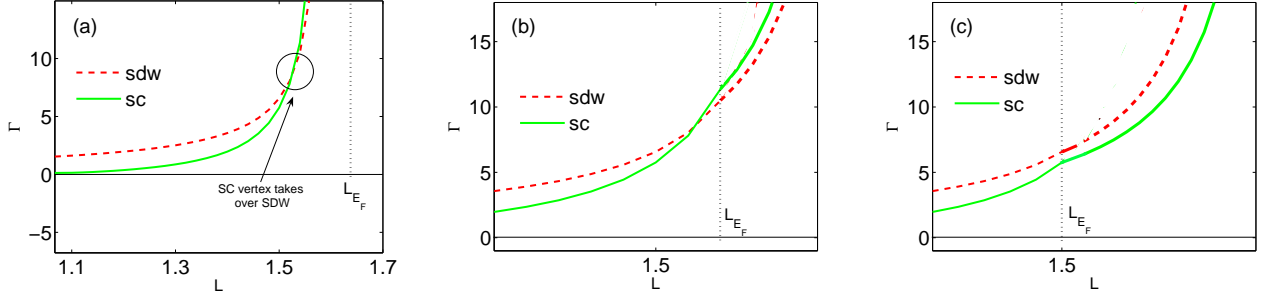


FIG. 12: The flow of vertices for different values of  $L_{E_F}$  for  $\alpha = 0.4$ . (a) RG flow reaches fixed point before  $L_{E_F}$ . SDW vertex is larger at small  $L$ , but SC vertex ‘crosses’ the SDW vertex at some distance from the fixed point and becomes the strongest vertex at the fixed point. As a result, the system develops a SC order. (b)  $L_{E_F}$  is reached after the ‘crossing’ but before reaching fixed point. The system still develops a SC order, and SDW order does not emerge. (c)  $L_{E_F}$  is reached before the ‘crossing’. In this case the SDW vertex still develops at small dopings, and SC order emerges at larger dopings, when SDW order gets suppressed.

on  $\alpha$  and on the interplay between  $E_F$  and the scale at which parquet RG flow reaches the fixed point.

#### 4. Effect of the angular dependence of electron-electron interaction

For completeness, we present the results for the evolution of the SC gap structure under RG flow for the case when we preserve the angular dependence in the electron-electron interactions –  $u_4$  and  $u_8$  terms. These interactions only contribute to the pairing channel, so it will be sufficient to consider  $u_4$  and  $u_8$  interactions between fermions with momenta  $k, -k; p, -p$ . The generic structure of the angular dependence of such interactions is given by Eq. (6). We found earlier that  $u_4$  and  $u_8$  terms contribute to the  $s$ -wave pairing in the combina-

tion  $\tilde{u}_4 = u_4 + u_8$ , so we need to consider only this term. We have

$$\tilde{u}_4(k, p) = \tilde{u}_4 \left( 1 + 2\alpha' (\cos 2\phi_k \pm \cos 2\phi_p) \pm 4\alpha'' \cos 2\phi_k \cos 2\phi_p \right) \quad (23)$$

where plus sign is for intra-pocket interaction and minus sign is for inter-pocket interaction.

There are two new effects associated with the angular dependence of  $\tilde{u}_4(k, p)$ . First, when  $\tilde{u}_4 u_5 > 2u_3^2$ , the pairing vertex  $\Gamma^{SC}$  not necessarily has an attractive component. It was always the case for angle-independent  $\tilde{u}_4$ . Now the existence of the attractive interaction is subject to condition  $K > 0$ , where

$$K = 2\tilde{u}_4 u_5 ((\alpha')^2 - \alpha'') + u_3^2 (\alpha^2 + 2\alpha'' - 3\alpha\alpha'). \quad (24)$$

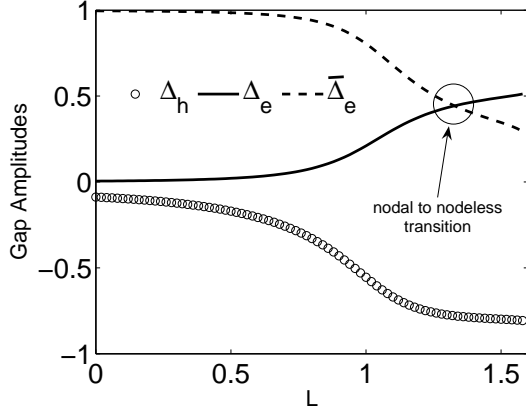


FIG. 13: The evolution of the three components of the superconducting gap with  $L$  for  $\alpha = 0.4$ .  $\Delta_h$  is the gap on the hole FS, and  $\Delta_e \pm \bar{\Delta}_e \cos 2\phi$  are the gaps along electron FSs. A circle marks the point where  $\Delta_e$  and  $\bar{\Delta}_e$  cross, and the gap along each of electron FSs changes from nodal to nodeless. Note that the solution is always of  $s\pm$  character; meaning  $\Delta_h$  and  $\Delta_1^e$  are of opposite signs.

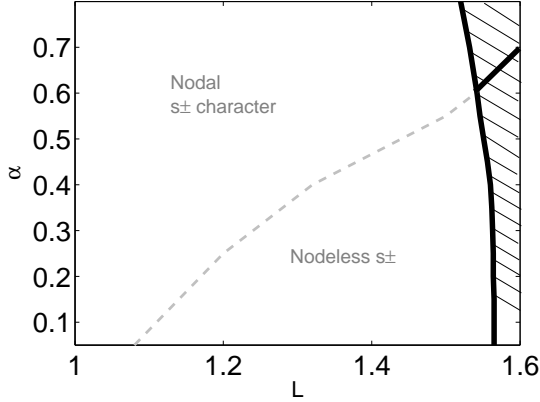


FIG. 14: The RG flow of the 4-pocket model in variables  $\alpha$  and  $L$  over the range of energies above  $E_F$ . The white zone is where SDW vertex is the largest, and the shaded zone is where SC  $s\pm$  vertex is the largest. The thick solid line in the shaded zone marks the transition from nodal to nodeless  $s\pm$  gap in the region where SC vertex wins. The dashed line is the continuation of this transition line into the region where SDW vertex takes over.

If we set the angular dependence of  $u_3$  and  $\tilde{u}_4$  terms to be equal, i.e., set  $\alpha' = \alpha, \alpha'' = 0$ , this condition reduces to  $\tilde{u}_4 u_5 > u_3^2$ , which is well satisfied. However, for a generic  $\alpha'$  and  $\alpha''$ , Eq. (24) is not necessarily satisfied, and if  $K < 0$ , attractive  $\Gamma_1^{SC}$  appears only above some RG scale  $L$ , like in 2-pocket model.

Second, the gap structure may change in some range of  $L$ . To demonstrate this, make angular dependence of  $u_3$  and  $\tilde{u}_4$  equal, i.e., set  $\alpha' = \alpha, \alpha'' = 0$ . The set of

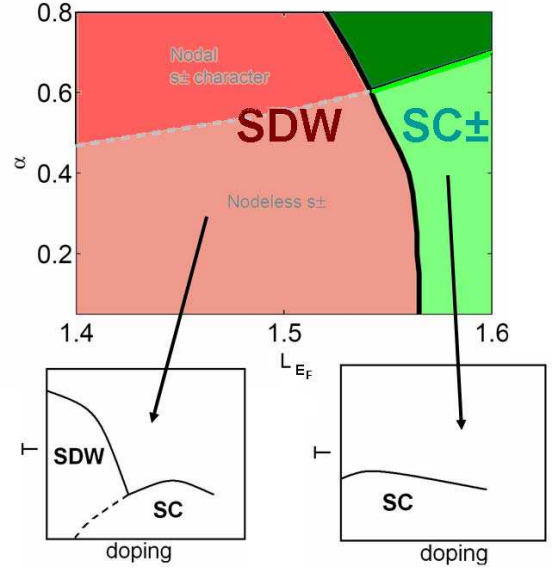


FIG. 15: The phase diagram of the 4-pocket model at perfect nesting in variables  $\alpha$  and  $L_{E_F} = \log \Lambda/E_F$ . In red is the region where SDW order develops, and in green is the region of the SC order. Dark and light green regions correspond to nodal (dark) and nodeless (light) SC gap along the electron FSs. The two sub-figures show the behavior at finite doping. Superconducting state which is brought out upon doping in the left sub-figure is either nodeless or nodal depending on the location with respect a dashed line inside the red (SDW) region. The transition between SDW and SC states can be either first order or involve intermediate co-existence phase<sup>58,59</sup>.

equations for the SC vertices then becomes

$$\begin{pmatrix} 1 - u_5 L & -2u_3 L & -2\alpha u_3 L \\ -u_3 L & 1 - \tilde{u}_4 L & -\alpha \tilde{u}_4 L \\ -2\alpha u_3 L & -2\alpha \tilde{u}_4 L & 1 \end{pmatrix} \begin{pmatrix} \Delta_h^o \\ \Delta_e^o \\ \bar{\Delta}_e^o \end{pmatrix} = \begin{pmatrix} \Delta_h \\ \Delta_e \\ \bar{\Delta}_e \end{pmatrix} \quad (25)$$

As before, we need to diagonalize this set, cast the result in the form  $\Delta_i = \Delta_i^o (1 + \Gamma_i L)$  and consider the largest  $\Gamma_i$ . The evolution with  $L$  of  $\Delta_h$ ,  $\Delta_e$ , and  $\bar{\Delta}_e$  for such  $\Gamma_i$  is shown in Fig 16, and the phase diagram is shown in Fig. 17. We see that, over some range when  $\bar{\Delta}_e$  is the largest and the gap has nodes along the electron FSs, the gap actually has "nodal  $s++$ " character in the sense that  $\Delta_h$  and  $\Delta_e$  are of the same sign, although the dominant term is still the oscillating component  $\bar{\Delta}_e$ . Note, however, that the character of the gap changes back to  $s\pm$  before it becomes nodeless.

This appearance of the nodal  $s++$  like gap might seem unusual, but it should be kept in mind that this gap is present in the parameter range where without the angular dependence there wouldn't have been a solution. The firm requirement then is that in the solution induced by  $\alpha$  the oscillating  $\bar{\Delta}_e$  component is the largest, because this is the way to minimize the effect of intra-pocket Coulomb repulsion. The relative sign between the subleading  $\Delta_h$  and  $\Delta_e$  terms is not uniquely determined by this requirement and be either minus or plus, depending on the in-

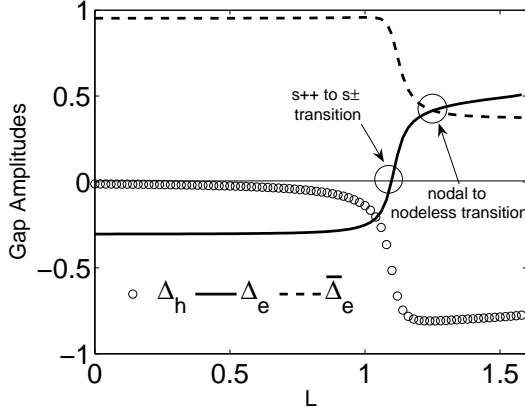


FIG. 16: Behavior of the different  $\Delta$ 's when the angular dependence of the electron intra-pocket coupling  $u_4$  is included. As before, we set  $\alpha = 0.4$ . The only difference compared to Fig. 13 is the appearance of the region, at small  $L$ , where SC order parameter has nodal  $s++$  character meaning that  $\Delta_h$  and  $\Delta_e$  are of the same sign. In this range of  $L$  the SC vertex is, however, smaller than the SDW vertex. The character of the SC gap changes to nodal  $s\pm$  and then to no-nodal  $s\pm$  before SC vertex takes over SDW vertex.

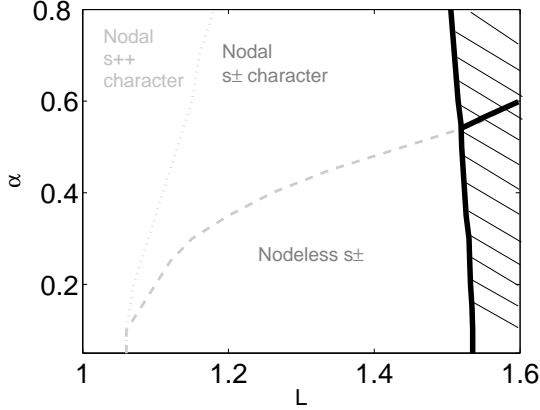


FIG. 17: Same as in Fig. 14, but with the angular dependence of the electron intra-pocket coupling  $u_4$  included. The only new feature is the existence of a range where SC vertex (secondary in this range to SDW vertex) has nodal  $s++$  character meaning that the gaps along electron FSs have nodes, but the average value of the gap along the electron FS is of the same sign as the gap along the hole FS.

terplay between electron-hole and electron-electron interactions.

These two potential changes introduced by the angular dependence of  $\tilde{u}_4$ , however, affect only the behavior at small  $L$ . At large  $L$  (i.e., at low energies), the system behavior remains unchanged: SDW vertex is the largest at small/intermediate  $L$ , but SC vertex still crosses over SDW vertex at some  $L$ , and beyond this scale SC instability comes first.

## B. The 4-pocket model in the limit when two hole FSs are identical

We now consider the opposite limit where the two hole FSs centered at  $(0,0)$  are equivalent. We show that the system behavior in this second limit is the same as in the first. The equivalence of the two limits hints that the system behavior in the intermediate case is very likely the same as in the two limits.

The computations in the case of two identical hole FSs proceed in the same way as before, but there are more vertices. The new terms are  $u_1, u_2$ , and  $u_3$  interactions with hole fermions from the second hole bands, the analogs of these three interactions for fermions from the two hole bands,  $u_5$  interaction for the second hole band, and the interactions of the kind  $u_5^* \sum c_1^\dagger c_1^\dagger c_1 c_2$ . Note that there are no  $f_1^\dagger f_1^\dagger f_1 f_2$  terms for fermions from the two electron bands because they would violate momentum conservation.

The full set of RG equations is rather cumbersome, but we verified that (i) RG flow indeed preserved the invariance between the two hole bands, and (ii) all intra-pocket and inter-pocket interactions involving fermions from the hole bands flow to the same value  $u_5$ . The analysis based on 5-orbital Hubbard model also yields near-equivalence of all  $u_i$  involving fermions from hole pockets<sup>61</sup>.

To simplify the presentation we set all interactions involving fermions near hole FSs to be equal to  $u_5$  from the start and also neglect the angular dependence of the interactions. We also set  $u_4 = u_8$  because  $u_4 - u_8 > 0$  again flows to zero under RG (see paragraph before Eq. 21).

### 1. The Vertices

The equations for the SC and SDW vertices are obtained in the same way as before (see Fig. (8)), but now  $\Delta_h$  is composed from fermions with  $k$  and  $-k$  belonging to either of the two hole pockets. This leads to the equations for the SDW vertex  $\Delta_1$  and SC vertices  $\Delta_h$  and  $\Delta_e$  in the form

$$\Delta_1 = \Delta_1^o (1 + \tilde{u}_1 + \tilde{u}_3) \quad (26)$$

and

$$\begin{pmatrix} 1 - \tilde{u}_5 L & -\tilde{u}_3 L \\ -2\tilde{u}_3 L & 1 - \tilde{u}_4 L \end{pmatrix} \begin{pmatrix} \Delta_h^o \\ \Delta_e^o \end{pmatrix} = \begin{pmatrix} \Delta_h \\ \Delta_e \end{pmatrix} \quad (27)$$

where  $\tilde{u}_1 = 2u_1$ ,  $\tilde{u}_3 = 2u_3$ ,  $\tilde{u}_4 = 2u_4$  and  $\tilde{u}_5 = 4u_5$ . Casting the results into  $\Delta_i = \Delta_i^o (1 + \Gamma_i L)$ , we obtain

$$\begin{aligned} \Gamma^{SDW} &= \tilde{u}_1 + \tilde{u}_3 \\ \Gamma^{s\pm} &= \frac{-(\tilde{u}_4 + \tilde{u}_5) + \sqrt{(\tilde{u}_4 - \tilde{u}_5)^2 + 8(\tilde{u}_3)^2}}{2} \end{aligned} \quad (28)$$



## 2. Parquet RG equations

The RG equations are obtained in the same way as before and are

$$\begin{aligned}\dot{\tilde{u}}_5 &= -[\tilde{u}_5^2 + 2\tilde{u}_3^2] \\ \dot{\tilde{u}}_4 &= -[\tilde{u}_4^2 + 2\tilde{u}_3^2] \\ \dot{\tilde{u}}_1 &= +[\tilde{u}_1^2 + \tilde{u}_3^2] \\ \dot{\tilde{u}}_3 &= +[4\tilde{u}_1\tilde{u}_3 - \tilde{u}_5\tilde{u}_3 - \tilde{u}_4\tilde{u}_3]\end{aligned}\quad (29)$$

We drop  $u_2$  for simplicity as it eventually becomes smaller than other  $u_i$

Comparing these equations and the equations for the vertices with those for one hole FS (Eqs. 18 and 21) we see that they are identical up to renormalizations  $u_i \rightarrow \tilde{u}_i$ . Accordingly, the flow of the couplings and the vertices is the same as in the limit when only one hole FS is present. In both limits, SC vertex is secondary to SDW vertex at large energies, but has larger slope and crosses over SDW vertex at some energy, before the system reaches a fixed point. At smaller energies, SC vertex is larger, i.e. if parquet RG flow extends beyond the scale where the two vertices cross, the system first develops a SC order even at perfect nesting. This SC order can be either with or without nodes in the gaps along the two electron FSs (see Fig. 15). The only difference to the effective 3-pocket model is that now at the fixed point we have  $\Delta_e = -\sqrt{2}\Delta_h$  for  $\alpha = 0$  as opposed to  $\Delta_h = -\sqrt{2}\Delta_e$  for the earlier case.

As we said, the equivalence of the system behavior in the two limits strongly suggests that the same behavior holds also in the intermediate case.

### C. Summary of the results for the 4-pocket model

Collecting all the points we have discussed – we have shown that under suitable extent of renormalization of the Coulomb repulsion and pair-hopping couplings one can have SDW, nodal  $s\pm$ , and nodeless  $s\pm$  state even at perfect nesting. The angular dependence of the interaction between holes and electrons tends to drive the system towards a nodal SC phase. The SC order develops if the fixed point is reached within parquet RG, but if the scale  $E_F$  is reached before that, the system develops either SDW or SC order (either nodeless or nodal), depending on at what  $L$  the flow crosses over from parquet to ladder RG. That the SC  $s\pm$  order can emerge even at perfect nesting is specific feature of the 4-pocket model. This feature was not present in the 2-pocket model, where the fixed point had an  $O(6)$  symmetry. This symmetry is clearly broken in the 4-pocket model, even when  $\alpha = 0$ . The ‘crossing’ of the SDW and SC vertices can be unambiguously attributed to the presence of the other electron pocket because its presence helps SC but not SDW.

Fig. 15 summarizes the implication of our results towards the actual phase diagrams of Fe-pnictides. In the

SDW dominated region (red), SC emerges after doping reduces SDW order. In the other part where SC dominates, SC order prevails already at perfect nesting. The  $s\pm$  SC gap can be nodeless or have nodes along electron FSs depending on how strong is the angular dependence of the interaction between electrons and holes.

*A final remark:* In the analysis above we considered only the interactions which obey momentum conservation in the unfolded BZ. These are direct interactions between fermionic states obtained by the hybridization of 5 *Fe* orbitals. There exists, however, additional interactions which involve pnictide orbitals as intermediate states. These additional interactions obey momentum conservation in the folded BZ, but they do not always obey momentum conservation in the unfolded, *Fe*-only BZ. An example of such process is shown in Fig. 18: two fermions from the hole band near  $k = 0$  scatter into two fermions at two *different* electron pockets. In the unfolded zone, this process doesn’t conserve momentum, and we didn’t include it into our consideration. In the folded zone, both electron FSs are at  $(\pi, \pi)$ , and this process is an umklapp process. The difference is indeed due to the fact that in reality such process involves intermediate states on As.

Neither our RG procedure nor fRG calculations include such terms. How important are they is not known. On general grounds, such interactions tend to enhance the SDW vertex and might potentially alter the picture that we presented. They also may alter the ordering momentum of the SDW state. This remains an open issue.

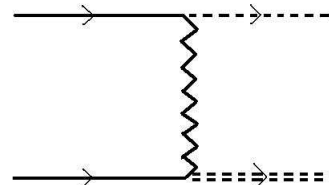


FIG. 18: The scattering which takes two fermions from the region near  $k = 0$  and scatters them to fermions with momenta near  $(\pi, 0)$  and  $(0, \pi)$ . This process is not allowed in the unfolded BZ because of momentum non-conservation, but it is allowed as an umklapp process in the folded BZ, which knows about As.

## V. 5-POCKET MODEL

We now extend the analysis from previous two sections to a 5-pocket model in which we include into consideration the additional hole pocket appearing at  $(\pi, \pi)$  point in the unfolded BZ. We show below that the behavior of 5-pocket model is similar to that for 2-pocket model in the sense that SDW vertex exceeds SC vertex along the whole RG trajectory, and SDW and SC vertices tend to the same value if the fixed point is reached within parquet RG.

As in the previous section, we restrict our consideration to the two limits, one when the two hole FSs centered at  $(0,0)$  are identical, and the other when one of these two hole FSs is relatively weakly coupled to electronic states and can be neglected. In the latter case, 5-pocket model reduces to an effective 4-pocket model consisting of one hole FS at  $(0,0)$ , one hole FS at  $(\pi,\pi)$ , and the two electron FSs at  $(0,\pi)$  and  $(\pi,0)$ . We show that the system behavior is again identical in the two limits.

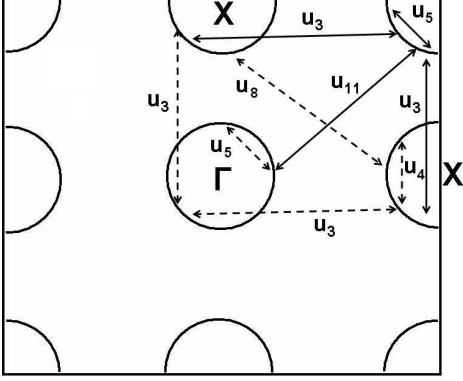


FIG. 19: The FSs and interactions in the 5-pocket model. Dashed lines mark the interactions already present in 4-pocket model, solid lines mark the new pairing interactions specific to 5-pocket model. As before, we only present interactions which contribute to the pairing vertices. There are other density-density and exchange interactions between electrons belonging to different pockets.

### A. Effective model with one hole pocket at $(0,0)$

The FS geometry and interactions contributing to the SC vertex for the effective 4-pocket model with hole pockets at  $(0,0)$  and  $(\pi,\pi)$  are presented in Fig. 19

The Hamiltonian now contains three new terms  $u_9$ ,  $u_{10}$ , and  $u_{11}$ , which are density-density, exchange, and pair-hopping interaction between fermions belonging to two different hole pockets. In addition, we have three new vertices shown in Fig. 20. These include fermions from two different hole and two different electron FSs. We call them  $w_i$  vertices ( $i$  runs from 1 to 3).

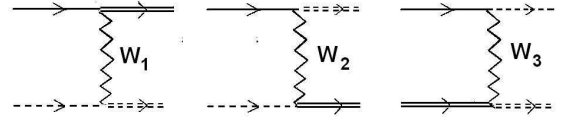


FIG. 20: The new interaction vertices for the 5-pocket model. Single and double solid lines denote fermions from the two hole pockets, single and double dashed lines denote fermions from the two electron pockets.

The Hamiltonian now has the form

$$\begin{aligned}
\frac{m}{2\pi} H_{int} = & \sum u_1^{(1)} c_{1p_1s}^\dagger f_{1p_2s'}^\dagger f_{1p_4s'} c_{1p_3s} + \sum u_2^{(1)} c_{1p_1s}^\dagger f_{1p_2s'}^\dagger c_{1p_4s'} f_{1p_3s} + \sum \frac{u_3^{(1)}}{2} \left( c_{1p_1s}^\dagger c_{1p_2s'}^\dagger f_{1p_4s'} f_{1p_3s} + h.c. \right) \\
& + f_1 \leftrightarrow f_2 \text{ (with } c_1 \text{ unchanged) and } u_i^{(1)} \leftrightarrow u_i^{(2)} + c_1 \leftrightarrow c_2 \text{ (with } f_1 \text{ unchanged) and } u_i^{(1)} \leftrightarrow u_i^{(3)} \\
& + c_1 \leftrightarrow c_2 \text{ (with } f_2 \text{ unchanged) and } u_i^{(2)} \leftrightarrow u_i^{(4)} \\
& + \sum \frac{u_4^{(1)}}{2} f_{1p_1s}^\dagger f_{1p_2s'}^\dagger f_{1p_4s'} f_{1p_3s} + \sum \frac{u_4^{(2)}}{2} f_{2p_1s}^\dagger f_{2p_2s'}^\dagger f_{2p_4s'} f_{2p_3s} \\
& + \sum \frac{u_5^{(1)}}{2} c_{1p_1s}^\dagger c_{1p_2s'}^\dagger c_{1p_4s'} c_{1p_3s} + \sum \frac{u_5^{(2)}}{2} c_{2p_1s}^\dagger c_{2p_2s'}^\dagger c_{2p_4s'} c_{2p_3s} \\
& + \sum u_6 f_{1p_1s}^\dagger f_{2p_2s'}^\dagger f_{2p_4s'} f_{1p_3s} + \sum u_7 f_{1p_1s}^\dagger f_{2p_2s'}^\dagger f_{1p_4s'} f_{2p_3s} + \sum \frac{u_8}{2} \left( f_{1p_1s}^\dagger f_{1p_2s'}^\dagger f_{2p_4s'} f_{2p_3s} + h.c. \right) \\
& + c \leftrightarrow f \text{ and } (u_6, u_7, u_8) \leftrightarrow (u_9, u_{10}, u_{11}) \\
& + \sum w_1 c_{1p_1s}^\dagger f_{1p_2s'}^\dagger f_{2p_4s'} c_{2p_3s} + \sum w_2 c_{1p_1s}^\dagger f_{1p_2s'}^\dagger c_{2p_4s'} f_{2p_3s} + \sum \frac{w_3}{2} c_{1p_1s}^\dagger c_{2p_2s'}^\dagger f_{1p_4s'} f_{2p_3s} + (1 \leftrightarrow 2) \quad (30)
\end{aligned}$$

The analysis of the 5-pocket model parallels that of the 4-pocket model, so we will be rather brief and present only the results. We verified that RG equations for  $u_4, u_5, u_8$  and  $u_{11}$  are identical, and these four couplings tend to the same value at the fixed point. To make the presentation compact, we set  $u_4 = u_5 = u_8 = u_{11}$

from the start and call all of them  $u_4$ . Similarly we set  $u_6 = u_7 = u_9 = u_{10}$  calling it  $u_6$ . It is convenient to introduce  $\tilde{u}_i = u_i + w_i$  ( $i = 1-3$ ), and  $\tilde{u}_i = u_i - w_i$ . We will use these variables below.

### 1. The Vertices

We first consider the case when the interactions are angle-independent ( $\alpha = 0$ ) and then discuss system behavior at a nonzero  $\alpha$ .

The SC and SDW vertices are obtained in the same way as before, but there are additional terms for the SDW term due to  $w_i$  vertices (see Fig. 21). Combining this with the equations for the SC vertices at  $(0, 0)$  and  $(\pi, \pi)$  ( $\Delta_{h1}$  and  $\Delta_{h2}$  respectively) we obtain

$$\begin{pmatrix} 1 - 2u_4L & -u_3L & -u_3L \\ -2u_3L & 1 - u_4L & -u_4L \\ -2u_3L & -u_4L & 1 - u_4L \end{pmatrix} \begin{pmatrix} \Delta_e^o \\ \Delta_{h1}^o \\ \Delta_{h2}^o \end{pmatrix} = \begin{pmatrix} \Delta_e \\ \Delta_{h1} \\ \Delta_{h2} \end{pmatrix} \quad (31)$$

and

$$\Delta_1 = \Delta_1^o(1 + (\tilde{u}_1 + \tilde{u}_3)L) \quad (32)$$

(we recall that we set  $u_4 = u_5$ ). Casting the equations for the SC vertices in the form  $\Delta_i = \Delta_i^o(1 + \Gamma_i)$  and neglecting repulsive vertex for  $s^{++}$  SC, we obtain

$$\begin{aligned} \Gamma^{SDW} &= \tilde{u}_1 + \tilde{u}_3 \\ \Gamma^{s^\pm} &= -2u_4 + \tilde{u}_3 + \tilde{\tilde{u}}_3 \end{aligned} \quad (33)$$

Note that SDW and SC vertices contain different terms involving  $u_3$ . The gap structure for the SC vertex  $\Gamma^{s^\pm}$  is  $\Delta_{h1} = \Delta_{h2} = -\Delta_e$ .

### 2. RG flow between $\Lambda$ and $E_F$

The set of parquet RG equations is obtained in the same way as before. Collecting the equations for the other variables we obtain

$$\begin{aligned} \dot{\tilde{u}}_1 &= \tilde{u}_1^2 + \tilde{u}_3^2 \\ \dot{\tilde{u}}_2 &= 2\tilde{u}_1\tilde{u}_2 - 2\tilde{u}_2^2 \\ \dot{\tilde{u}}_3 &= 4\tilde{u}_1\tilde{u}_3 - 2\tilde{u}_2\tilde{u}_3 - 2\tilde{u}_3(u_4 + u_6) - 2\tilde{\tilde{u}}_3(u_4 - u_6) \\ 2\dot{u}_6 &= -(2u_6)^2 - (\tilde{u}_3 - \tilde{\tilde{u}}_3)^2 \\ 2\dot{u}_4 &= -(2u_4)^2 - (\tilde{u}_3 + \tilde{\tilde{u}}_3)^2 \\ \dot{\tilde{u}}_3 &= 4\tilde{\tilde{u}}_1\tilde{\tilde{u}}_3 - 2\tilde{\tilde{u}}_2\tilde{\tilde{u}}_3 - 2\tilde{\tilde{u}}_3(u_4 + u_6) - 2\tilde{\tilde{u}}_3(u_4 - u_6) \\ \dot{\tilde{\tilde{u}}}_1 &= \tilde{\tilde{u}}_1^2 + \tilde{\tilde{u}}_3^2 \\ \dot{\tilde{\tilde{u}}}_2 &= 2\tilde{\tilde{u}}_1\tilde{\tilde{u}}_2 - 2\tilde{\tilde{u}}_2^2 \end{aligned} \quad (34)$$

This set of equations almost decouples between the subsets for  $\tilde{u}_i$  and  $\tilde{\tilde{u}}_i$ , the only places where the two subsets mix are the equations for the flow of  $u_4$  and  $u_6$  whose r.h.s. contains both  $\tilde{u}_3$  and  $\tilde{\tilde{u}}_3$ . Re-writing this set as equations for the ratios of the couplings, we found four fixed points. One corresponds to  $\tilde{u}_i$  vanishing compared to  $\tilde{\tilde{u}}_i$ , another to  $\tilde{\tilde{u}}_i$  vanishing compared to  $\tilde{u}_i$ , the third corresponds to  $\tilde{u}_3 = \tilde{\tilde{u}}_3$ ,  $\tilde{u}_1 = \tilde{\tilde{u}}_1$ , and the fourth corresponds to  $\tilde{u}_3 = -\tilde{\tilde{u}}_3$ ,  $\tilde{u}_1 = \tilde{\tilde{u}}_1$ . The first two fixed points

are attractive, the other two are saddle points. Which fixed point the system will flow to depends on the initial conditions. In our case all interactions are positive (repulsive), i.e. at the bare level  $\tilde{u}_i$  are all positive and  $\tilde{u}_i > \tilde{\tilde{u}}_i$ . For these initial conditions, we verified that the system is outside the base of attraction of the second fixed point as it can be reached only if bare  $w_i$  are negative (at this fixed point  $\tilde{u}_i$  vanishes compared to  $\tilde{\tilde{u}}_i$  i.e.,  $w_i/u_i$  tends to  $-1$ ).

At the first attractive fixed point  $\tilde{\tilde{u}}_i$  vanishes compared to  $\tilde{u}_i$  i.e.,  $w_i/u_i$  tends to 1. This is consistent with our initial conditions. Near this fixed point,  $\tilde{\tilde{u}}_3$  can be neglected compared to  $\tilde{u}_3$  in the equations for  $\dot{u}_4$  and  $\dot{u}_6$ , and the first five RG equations form a closed set:

$$\begin{aligned} \dot{\tilde{u}}_1 &= \tilde{u}_1^2 + \tilde{u}_3^2 \\ \dot{\tilde{u}}_2 &= 2\tilde{u}_1\tilde{u}_2 - 2\tilde{u}_2^2 \\ \dot{\tilde{u}}_3 &= 4\tilde{u}_1\tilde{u}_3 - 2\tilde{u}_2\tilde{u}_3 - 2\tilde{u}_3(u_4 + u_6) \\ 2\dot{u}_4 &= -(2u_4)^2 - \tilde{u}_3^2 \\ 2\dot{u}_6 &= -(2u_6)^2 - \tilde{u}_3^2 \end{aligned} \quad (35)$$

Within the same approximation

$$\begin{aligned} \Gamma^{SDW} &= \tilde{u}_1 + \tilde{u}_3 \\ \Gamma^{s^\pm} &= -2u_4 + \tilde{u}_3 \end{aligned} \quad (36)$$

Comparing these equations with the ones we obtained for the 2-pocket model, Eqs. (10) and (11), we see that they are equivalent, up to overall renormalizations of the couplings, if we identify  $2u_6$  in Eq. (35) with  $u_5$  in Eq. (11). There is minor difference between the  $\Gamma^{s^\pm}$  in the two cases ( $2u_4$  in (36) vs  $u_4 + u_5$  in (10)), but it vanishes at the fixed point. Accordingly, the RG flow of the couplings and the vertices is the same as in the 2-pocket model, namely SDW vertex remains dominant for all  $L$  up to a fixed point, and SC vertex changes sign at some  $L$ , becomes attractive at larger  $L$  and becomes equal to the SDW vertex at the fixed point if, indeed, the fixed point is reached within parquet RG. This similarity with a 2-pocket model was first noted by K. Haule<sup>60</sup> and can be understood if we note that in the 5 pocket case SC pairing is the same as in 4-pocket model (with extra combinatoric factor of 2 compared to 2-pocket case), but SDW pairing is now possible between the two sets of electron pockets (see Fig. 21), this adds the combinatoric factor of 2 also to the renormalization of the SDW vertex.

We now need to understand what is the basis of attraction for this fixed point. For this, we consider the two other fixed points for which  $\tilde{u}_3 = \tilde{\tilde{u}}_3$ ,  $\tilde{u}_1 = \tilde{\tilde{u}}_1$ , or  $\tilde{u}_3 = -\tilde{\tilde{u}}_3$ ,  $\tilde{u}_1 = \tilde{\tilde{u}}_1$ . We show that both are saddle points, and both are unstable when the bare  $u_i$  and  $w_i$  are all positive.

Consider for example the fixed point at  $\tilde{\tilde{u}}_1 = \tilde{u}_1$  and  $\tilde{\tilde{u}}_3 = \tilde{u}_3$ . At this fixed point  $u_4/\tilde{u}_1 = -3$ ,  $\tilde{u}_3/\tilde{u}_1 = \sqrt{15}$  and  $u_6 = 0$ . Expanding in  $\delta = \tilde{u}_1 - \tilde{\tilde{u}}_1$  and  $\epsilon = \tilde{u}_3 - \tilde{\tilde{u}}_3$ , we obtain the set of coupled linear differential equations

$$\begin{aligned}\dot{\delta} &= 2\tilde{u}_1 (\delta + \sqrt{15}\epsilon) \\ \dot{\epsilon} &= 4\tilde{u}_1 (\sqrt{15}\delta + 4\epsilon)\end{aligned}\quad (37)$$

together with  $\dot{\tilde{u}}_1 = \tilde{u}_1^2 + \tilde{u}_3^2 = 16\tilde{u}_1^2$ . The solution of the set is  $\epsilon = \epsilon_0 (\tilde{u}_1)^\gamma$ ,  $\delta = \delta_0 (\tilde{u}_1)^\gamma$ . Substituting and solving for the set of two linear equations for  $\epsilon_0$  and  $\delta_0$ , we obtain  $\gamma_1 = 11/8$  and  $\gamma_2 = -1/4$ . For  $\epsilon$  and  $\delta$  which correspond to  $\gamma = \gamma_1$ , the fixed point is unstable, for  $\gamma = \gamma_2$ , it is stable. A simple analysis shows that  $\gamma_1$  is the solution when  $\epsilon_0/\delta_0 > 0$ , while  $\gamma_2$  is the solution when  $\epsilon_0/\delta_0 < 0$ . In our case, the bare values of  $\epsilon$  and  $\delta$  are  $2w_3$  and  $2w_1$ , respectively, both are positive. Hence this fixed point is unstable, and the RG flow bring the system towards the stable fixed point at which  $\tilde{u}_1$  and  $\tilde{u}_3$  are both small. The stability analysis of the fixed point at  $\tilde{u}_1 = \tilde{u}_1$ , or  $\tilde{u}_3 = -\tilde{u}_3$  yields the same results, leaving the fixed point with  $\tilde{u}_i \ll \tilde{u}_i$  as the only stable fixed point.

We next consider how the results are modified due to angular dependence of the vertices. We found two effects. First, one of SC vertices  $\Gamma_1^{SC}$  can become attractive already at small  $L$  in the same way as in the 3-pocket model studies in the previous section. Namely, the system adjusts  $\cos 2\phi$  and angle-independent components of the gaps along the two electron FSs to minimize the effect of intra-pocket Coulomb repulsion. Just as for 3-pocket model,  $\Gamma_1^{SC}$  is attractive and scales as  $\alpha^2$  if we only include angular dependence of the pair-hopping  $u_3$  and  $w_3$  terms. Second, SC and SDW vertices do not become identical at the fixed point if  $\alpha$  is nonzero. If we only include angular dependence of  $u_3, w_3$  and  $u_1$  and  $w_1$  (and set them equal), we find that SC vertex becomes larger than SDW vertex very near fixed point. However, the effect is numerically very weak, even when  $\alpha \sim 1$ . In Fig. 22 we show the flow of SC and SDW vertices for  $\alpha = 0.3$ . SC vertex eventually becomes larger, but this is truly weak effect.

The flow of SDW and SC vertices towards almost the same value in the 5-pocket model has been found numerically by Thomale et al within fRG study<sup>27</sup>. Our analytical RG results for this case again agree with their fRG, what, in our opinion, is another confirmation that the “topology” of the RG flow is chiefly determined by combinatoric effects.

### 3. RG flow below the scale of $E_F$

The system behavior for the case when the fixed point of the functional RG is not reached at  $E > E_F$  is quite similar to the 2-pocket model with the only difference that now SC instability always occurs when SDW order is destroyed by doping. Namely, at perfect nesting the system develops SDW order. At finite doping, the RG flow of the SDW vertex levels off, and SC vertex eventually becomes larger. The SC gap has  $\pm$  structure either

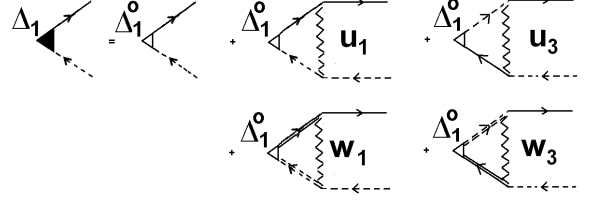


FIG. 21: The diagrammatic equation for the renormalized SDW vertex in the 5-pocket model. Comparing with the corresponding Fig. 8a for the 4-pocket case, there are extra diagrams which contribute to the SDW vertex. This leads to effectively doubling  $\Gamma^{SDW}$ .

without or with nodes along the electron FS, depending on the values of  $\alpha$  and of  $\log \Lambda/E_F$ . The phase diagram is similar to that in Fig. 15, but only has the “SDW” region in that figure.

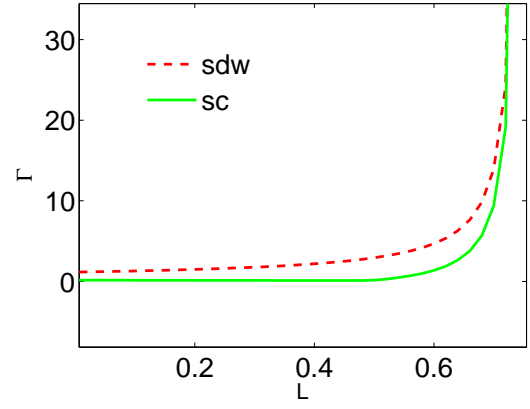


FIG. 22: Parquet RG flow of SC and SDW vertices for the 5-pocket model at  $\alpha = 0.3$ . The SDW vertex remains the largest over the whole flow, and the ratio of the SDW and SC vertices approaches one at the fixed point of parquet RG. This is very similar to the 2-pocket case except that here  $\Gamma^{SC}$  is attractive for all  $L$ .

### B. 5-pocket model with two equivalent hole FS at $(0,0)$

We now consider the opposite limit of 5-pocket model when the two hole pockets centered at  $(0,0)$  are equivalent. Our goal is to verify whether the system behavior remains the same as in the limit when we keep only one of these two hole pockets.

The computations in the case of two equivalent hole pockets at  $(0,0)$  are quite involved and we only present the results for  $\alpha = 0$ . Because the pockets at  $(0,0)$  and  $(\pi, \pi)$  are now non-equivalent (in the sense that there are two pockets at  $(0,0)$  and only one at  $(\pi, \pi)$ ), the interactions involving these pockets do not need to flow to the same value under RG, e.g.  $u_i$  and  $w_i$  need not to

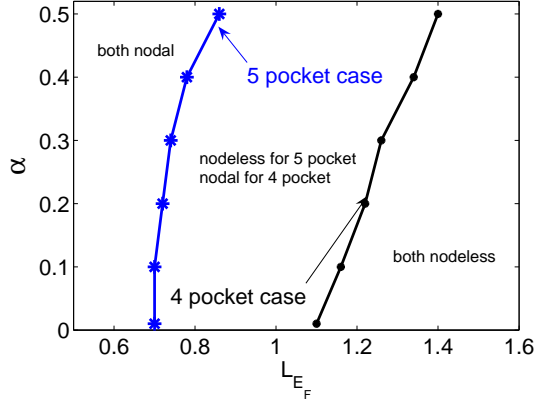


FIG. 23: Comparison of the SC phases for 4 and 5 pocket models. The initial conditions are identical for the common parameters. The figure shows that there exists a parameter range where the SC gap is nodeless in the 5-pocket model but is nodal in the 4-pocket model.

fly to the same value, and also electron-hole and hole-hole interactions involving fermions from near  $(0,0)$  and  $(\pi,\pi)$  need not to be the same. Finally, SC gaps on the hole FSs at  $(0,0)$  and  $(\pi,\pi)$  also do not have to be equal.

### 1. The Vertices

Keeping all this in mind and applying the same analysis as before we obtain the equations for the SDW and SC vertices. For the SDW, we introduce two vertices  $\Delta_1$  and  $\Delta_2$ , shown in Fig. 24 and write the set of  $2 \times 2$  coupled equations as

$$\begin{pmatrix} 1 + 2(u_1 + u_3)L & (w_1 + w_3)L \\ 2(w_1 + w_3)L & 1 + (\bar{u}_1 + \bar{u}_3)L \end{pmatrix} \begin{pmatrix} \Delta_1^o \\ \Delta_2^o \end{pmatrix} = \begin{pmatrix} \Delta_1 \\ \Delta_2 \end{pmatrix} \quad (38)$$

where the vertices  $\bar{u}_1$  and  $\bar{u}_3$  are shown in Fig. 25

For the SC vertex we introduce, as before,  $\Delta_e$ ,  $\Delta_{h1} = \Delta(k=(0,0))$  and  $\Delta_{h2} = \Delta(k=(\pi,\pi))$  and obtain

$$\begin{pmatrix} 1 - 2u_4L & -4u_3L & -\bar{u}_3L \\ -2u_3L & 1 - 4u_5L & -\bar{u}_5L \\ -2\bar{u}_3L & -4\bar{u}_5L & 1 - \bar{\bar{u}}_5L \end{pmatrix} \begin{pmatrix} \Delta_e^o \\ \Delta_{h1}^o \\ \Delta_{h2}^o \end{pmatrix} = \begin{pmatrix} \Delta_e \\ \Delta_{h1} \\ \Delta_{h2} \end{pmatrix} \quad (39)$$

The vertices  $\bar{u}_5$  and  $\bar{\bar{u}}_5$  are shown in Fig 25

### 2. Parquet RG equations

The total number of RG equations is quite large and we refrain from writing all of them. Quite predictably, the combinatoric factors associated with the existence of the two equivalent pockets at  $(0,0)$  give rise to relations  $\bar{u}_i = 2u_i$  ( $i = 1, 3, 5$ ),  $u_4 = 4u_5$ , and  $\bar{\bar{u}}_5 = 4u_5$ . Using these relations, we obtain for the relevant couplings  $u_1, w_1, u_3, w_3$  and  $u_4$  the set

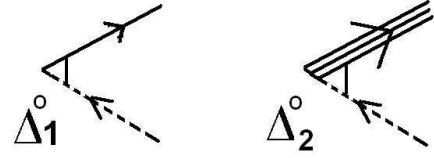


FIG. 24: The two non-equivalent SDW vertices in the 5-pocket model with two identical hole FSs at  $(0,0)$ . The triple solid line stands for the fermion (hole) at  $(\pi,\pi)$ . These two vertices are present also for the case when there is only one hole FSs at  $(0,0)$ , but in that case we set  $\Delta_1^o = \Delta_2^o$  and verified that the equivalence also holds for renormalized  $\Delta_{1,2}$ .

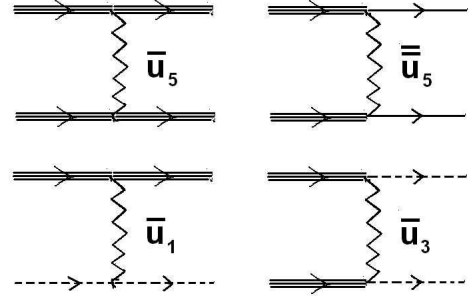


FIG. 25: The interactions involving fermions near the hole FS at  $(\pi,\pi)$  (the triple solid line). The dashed line stands for a fermion from an electronic pocket. For the case of only one hole FSs at  $(0,0)$  we set  $\bar{u}_5 = \bar{\bar{u}}_5 = u_5$ ,  $\bar{u}_1 = u_1$ , and  $\bar{u}_3 = u_3$  from the beginning and verified that these relations hold for running couplings. For the case of two identical hole pockets at  $(0,0)$ , the fixed point values of the couplings involving fermions near  $(\pi,\pi)$  are different from those involving fermions near  $(0,0)$ .

$$\begin{aligned} \dot{u}_1 &= 2(u_1^2 + u_3^2) + w_1^2 + w_3^2 \\ \dot{w}_1 &= 4w_1u_1 + 4w_3u_3 \\ \dot{u}_3 &= 4(2u_1u_3 + w_1w_3) - 4u_3u_4 \\ \dot{w}_3 &= 8(u_1w_3 + u_3w_1) - 4u_6w_3 \\ 2\dot{u}_4 &= -(2u_4)^2 - 16u_3^2 \\ 2\dot{u}_6 &= -(2u_6)^2 - 8w_3^2 \end{aligned} \quad (40)$$

Introducing now  $\tilde{u}_1 = 2u_1 + \sqrt{2}w_1$ ,  $\tilde{\tilde{u}}_1 = 2u_1 - \sqrt{2}w_1$ ,  $\tilde{u}_3 = 2u_3 + \sqrt{2}w_3$ ,  $\tilde{\tilde{u}}_3 = 2u_3 - \sqrt{2}w_3$  and substituting into (40) we obtain

$$\begin{aligned} \dot{\tilde{u}}_1 &= \tilde{u}_1^2 + \tilde{\tilde{u}}_3^2 \\ \dot{\tilde{u}}_3 &= 4\tilde{u}_1\tilde{u}_3 - 2\tilde{\tilde{u}}_3(u_4 + u_6) - 2\tilde{\tilde{u}}_3(u_4 - u_6) \\ 2\dot{\tilde{u}}_4 &= -(2u_4)^2 - (\tilde{u}_3 + \tilde{\tilde{u}}_3)^2 \\ 2\dot{\tilde{u}}_6 &= -(2u_6)^2 - (\tilde{u}_3 - \tilde{\tilde{u}}_3)^2 \\ \dot{\tilde{\tilde{u}}}_1 &= \tilde{\tilde{u}}_1^2 + \tilde{\tilde{u}}_3^2 \\ \dot{\tilde{\tilde{u}}}_3 &= 4\tilde{\tilde{u}}_1\tilde{\tilde{u}}_3 - 2\tilde{\tilde{u}}_3(u_4 + u_6) - 2\tilde{\tilde{u}}_3(u_4 - u_6) \end{aligned} \quad (41)$$

This is exactly the same set as Eq. (34) that we obtained in the previous subsection (we skip the equation on  $u_2$  which is irrelevant coupling anyway).

Under the same conditions ( $\bar{u}_i = 2u_i$  ( $i = 1, 3, 5$ ),  $u_4 = 4u_5$ , and  $\bar{\tilde{u}}_5 = 4u_5$ ), the relevant SDW and SC vertices become

$$\begin{aligned}\Gamma^{SDW} &= \tilde{u}_1 + \tilde{u}_3 \\ \Gamma^{s\pm} &= -2u_4 + \tilde{u}_3 + \tilde{\tilde{u}}_3\end{aligned}\quad (42)$$

These again are the same equations as Eqs (33) for the case of only one hole FS at  $(0,0)$ . The only difference with the other limit is that now the solutions corresponding to  $\Gamma^{SDW}$  and  $\Gamma^{s\pm}$  from (42) are  $\Delta_2 = \sqrt{2}\Delta_1$  and  $\Delta_{h2} = 2\Delta_{h1} = -\Delta_e$ .

We see therefore that the system behavior in the two limits is identical. Like in the 4-pocket case, this equivalence strongly suggests that the same behavior holds also in the intermediate, most generic 5-pocket model, when the two hole pockets at  $(0,0)$  are both present but are not identical.

### C. Summary of the results for 5-pocket model

We see that the system behavior in a 5-pocket model is “intermediate” between 2-pocket and 4-pocket models. On one hand, like in a 4-pocket model, the largest SC vertex can be positive already at the smallest  $L$ , even when intra-pocket Coulomb repulsion is the dominant interaction. If this is the case, then there is no critical  $L$  before which SC vertex is repulsive, and the system always becomes a SC when the competing SDW instability is reduced. The SC gap is either nodeless or with nodes on electron FSs, depending on  $\alpha$ , much like in the unshaded region in Fig. 14. On the other hand, like in a 2-pocket model, SDW vertex remains larger than SC vertex for all  $L$  before the fixed point is reached, and the two vertices flow to the same value at the fixed point of parquet RG (Fig. 22). This last statement is exact when  $\alpha = 0$  and remains numerically quite accurate even when  $\alpha \neq 0$  although strictly speaking, at a finite  $\alpha$ , SC vertex eventually becomes larger than SDW vertex in the immediate vicinity of the fixed point.

### D. Comparison of 4-pocket and 5-pocket models

It is instructive to compare the structures of the SC gaps in 5-pocket and 4-pocket models for the same values of input parameters (and using the same relations as above for extra parameters of a 5-pocket model). This comparison is shown in Fig. 23. We see that there is quite wide parameter range where in the 4-pocket model the gap has nodes while in the 5 pocket model it is still nodeless. Each point in the phase diagram in Fig. 23 corresponds to some values of the couplings, hence this result implies that for a certain range of input parameters

4-pocket model yields a gap with nodes while 5-pocket model yields the gap without nodes. This agrees with the number of RPA studies<sup>20,29,30</sup> which found nodal gap for 5-pocket model and no-nodal gap for 4 pocket model. At the same time, our results show that in both models there are regions of parameters in which the SC gap is either no-nodal or has nodes.

## VI. CONCLUSION

We have done calculations addressing on the same footing the issues of the interplay between intra and inter-pocket Coulomb repulsion in the Fe-based superconductors, the competition between SC and SDW orders, and the angular dependence of the SC gap. We considered 2-, 4-, and 5-pocket models for the pnictides and for each model considered the flow of the couplings and of SDW and SC vertices within analytical parquet RG scheme. We found that in all models, fluctuations in the SDW and SC channels are coupled at intermediate energies  $\Lambda > E > E_F$  between the bandwidth and the Fermi energy, but decouple at energies below  $E_F$ . The system behavior below  $E_F$  is governed by conventional ladder RG, and each vertex flows according to  $d\Gamma_i/dL = \Gamma_i^2$ .

For the toy 2-pocket model, earlier results showed<sup>22,51</sup> that SDW instability is the dominant one at perfect nesting. The SC vertex is repulsive at large energies but changes sign under parquet RG and become attractive above some RG scale. The SDW and SC couplings flow to the same value at the fixed point of RG equations, and the fixed point of parquet RG has extended  $O(6)$  symmetry.<sup>52</sup> If the scale of  $E_F$  is reached before this fixed point, SDW order prevails at zero doping but is reduced and eventually destroyed at finite doping. Whether or not SC appears in place of SDW order depends on whether SC vertex already changes sign and becomes attractive at  $E_F$ . If superconductivity appears, the SC gap has a simple plus-minus structure.

The main goal of this paper was to understand how this scenario is modified in realistic 4-pocket and 5-pocket models. We considered both models in the two limits: one when one of the two hole pockets centered at  $(0,0)$  is weakly coupled to other pockets and can be neglected, and the other when the two hole pockets centered at  $(0,0)$  are equivalent. We found identical results in both limit what gives us confidence that the system behavior in the intermediate case of two non-equivalent hole pockets at  $(0,0)$  remains the same as in the two limits.

Our main results are the following:

- In both 4-pocket and 5-pocket models electron-hole and electron-electron interactions are generally angle dependent. The most relevant angle dependence is in the form  $\cos 2\phi$ , where  $\phi$  is the angle along an electron FS. Because of this angular dependence, there are three different vertices in the SC channel. One of these vertices turns out to be

attractive, in most cases, beginning from the largest energies. The symmetry of the attractive interaction is extended  $s\pm$  wave (as opposed to a conventional  $s++$ ). Other two SC vertices are repulsive at all scales.

- This attractive SC vertex favors the  $s\pm$  state in which the gaps along hole FSs are angle-independent (up to  $\cos 4\phi$  corrections), while the gaps along the two electron FSs are in the form  $\Delta_e \pm \bar{\Delta}_e \cos 2\phi$ . The interplay between  $\Delta_e$  and  $\bar{\Delta}_e$  depends on the strength of  $\cos 2\phi$  component of the interaction and also on the interplay between intra-pocket and inter-pocket Coulomb repulsions. Depending on the parameters, the electron gaps can be either nodeless ( $\Delta_e > \bar{\Delta}_e$ ), or have accidental nodes ( $\Delta_e < \bar{\Delta}_e$ ).
- In 5-pocket model at perfect nesting, the SDW vertex remains larger than this attractive SC vertex. The two flow up to the same values at the fixed point, if this fixed point is at an energy larger than  $E_F$ , and the fixed point has enlarged symmetry. This behavior is exact when the vertices are angle-independent, but only very weakly changes due to angular dependence of the vertices. If the system flows down to  $E_F$  without yet reaching the fixed point, SDW order wins. Away from perfect nesting SDW order is suppressed, and the system eventually develops a SC instability.
- In 4-pocket model, the situation is similar at large  $E$  (i.e., at small RG parameter  $\log \Lambda/E$ ), but before the fixed point of parquet RG is reached, SC vertex becomes larger than SDW vertex. If this happens before the scale of  $E_F$  is reached, the system develops SC instability already at perfect nesting, and SDW instability does not appear. If SDW vertex remains the largest down to  $E_F$ , the system develops SDW instability at and around perfect nesting, and SC instability at larger dopings.
- We found that the SC gap is more likely to have accidental nodes on electron FSs in 4 pocket model than in 5-pocket model. Namely, for the same input parameters, there is a parameter range where the gap is nodal in 4-pocket model and no-nodal in 5-pocket model. This agrees with several RPA-type

studies based on spin fluctuations<sup>20,29,30</sup>. Still, we found that in both 4-pocket and 5-pocket model the gap can be either nodal or node-less, depending on parameters.

Our analytical results are fully consistent with numerical fRG study of 4-pocket and 5-pocket models by Thomale et al<sup>27</sup>. We view this agreement as the evidence that the differences between 4-pocket and 5-pocket models are geometrical (different combinatorics in RG equations), and are captured already within analytical one-loop RG. We note in this regard that we found that the difference between 4-pocket and 5-pocket models is not caused by the angular dependence of the interaction and holds even when interactions are angle-independent.

The results for the 4-pocket case demonstrate that SDW order need not be pre-requisite to  $SC\pm$  order, although for most part of the phase diagram it does appear at perfect nesting, and SC only appears upon doping. We also emphasize that the interplay between SC and SDW is both “mutual support” and “competition”. Namely, SC and SDW *fluctuations* tend to enhance each other, what is relevant is the fact that in the applicability range of parquet RG (when SC and SDW fluctuations talk to each other), both SC and SDW vertices diverge upon approaching the fixed point. At the same time, SDW and SC *orders* compete with each other<sup>58,59</sup>, meaning that SC order only emerges when SDW order is reduced enough by doping, and SDW order does not emerge at all if SC order emerges first already at perfect nesting.

### Acknowledgements

We acknowledge helpful discussions with L. Benfatto, R. Fernandes, W. Hanke, P. Hirschfeld, I. Eremin, Y. Matsuda, I. Mazin, R. Prozorov, D. Scalapino, J. Schmalian, Z. Tesanovic, R. Thomale, M. Vavilov, and A. Vorontsov. We also thank I. Mazin for careful reading of the MS and useful comments. This work was supported by NSF-DMR-0906953. Partial support from MPI PKS (Dresden) (S.M. and A.V.C), Ruhr-University Bochum (S.M), and Humboldt foundation (A.V.C) is gratefully acknowledged.

<sup>1</sup> For recent reviews see D.C. Johnston, Adv. Phys., **59**, 803 (2010); J-P Paglione and R.L. Greene, Nature Phys. **6**, 645 (2010).

<sup>2</sup> Y. Kamihara, T. Watanabe, M. Hirano, H. Hosono, J. Am. Chem. Soc. **130**, 3296(2008).

<sup>3</sup> X. H. Chen, T. Wu, G. Wu, R. H. Liu, H. Chen, D. F. Fang, Nature **453**, 761(2008).

<sup>4</sup> G. F. Chen, Z. Li, D. Wu, G. Li, W. Z. Hu, J. Dong, P.

Zheng, J. L. Luo, and N. L. Wang, Phys. Rev. Lett. **100**, 247002 (2008).

<sup>5</sup> Z.-A. Ren, *et. al.*, Europhys. Lett. **83**, 17002(2008)

<sup>6</sup> M. Rotter, M. Tegel, D. Johrendt, Phys. Rev. Lett. **101**, 107006 (2008)

<sup>7</sup> K. Sasmal, B. Lv, B. Lorenz, A. M. Guloy, F. Chen, Y.-Y. Xue, and C.-W. Chu, Phys. Rev. Lett. **101**, 107007 (2008),

<sup>8</sup> N. Ni, A. Thaler, J. Q. Yan, A. Kracher, E. Colombier, S.

- L. Bud'ko, P. C. Canfield, Phys. Rev. B **82**, 024519 (2010).
- <sup>9</sup> X. C. Wang, *et al.*, arXiv:0806.4688v3; S.V. Borisenko *et al* Phys. Rev. Lett. **105**, 067002 (2010).
- <sup>10</sup> Y. Mizuguchi, F. Tomioka, S. Tsuda, T. Yamaguchi, and Y. Takano, Appl. Phys. Lett. **93**, 152505 (2008), F. C. Hsu *et al.*, Proc. Natl. Acad. Sci. U.S.A. **105**, 14 262 (2008), M. H. Fang *et al.*, Phys. Rev. B **78**, 224503 (2008), G. F. Chen *et al.*, Phys. Rev. B **79**, 140509(R) (2009), B. Zeng *et al.*, arXiv:1007.3597.
- <sup>11</sup> C. de la Cruz *et al.*, Nature, **453**, 899 (2008). For the latest results on magnetic measurements, see D. S. Inosov, *et al.*, Nature Physics **6**, 178-181 (2010) and references therein.
- <sup>12</sup> Y. Kamihara *et al.*, J. Am. Chem. Soc. **128**, 10012 (2006).
- <sup>13</sup> M. Li *et al.* Phys. Rev. B **80**, 024515 (2009)
- <sup>14</sup> S.E. Sebastian *et al.*, J. Phys.: Condens. Matter **20** 422203(2008).
- <sup>15</sup> D.J. Singh and M.-H. Du, Phys. Rev. Lett. **100**, 237003 (2008); M.J. Calderon, B. Valenzuela, and E. Bascones, Phys. Rev. B **80**, 094531 (2009).
- <sup>16</sup> L. Boeri, O. V. Dolgov, and A. A. Golubov, Phys. Rev. Lett. **101**, 026403 (2008)
- <sup>17</sup> I. I. Mazin, D. J. Singh, M. D. Johannes, and M. H. Du, Phys. Rev. Lett. **101**, 057003 (2008)
- <sup>18</sup> Seiichiro Onari and Hiroshi Kontani, arXiv:1009.3882.
- <sup>19</sup> K. Kuroki *et al.*, Phys. Rev. Lett. **101**, 087004 (2008)
- <sup>20</sup> K. Kuroki, H. Usui, S. Onari, R. Arita, and H. Aoki, Phys. Rev. B **79**, 224511 (2009).
- <sup>21</sup> K. Seo, B. A. Bernevig, and J. Hu, Phys. Rev. Lett. **101**, 206404 (2008).
- <sup>22</sup> A. V. Chubukov, D. V. Efremov, and I. Eremin, Phys. Rev. B **78**, 134512 (2008).
- <sup>23</sup> V. Stanev, J. Kang, Z. Tesanovic, Phys. Rev. B **78**, 184509 (2008); V. Stanev, B. S. Alexandrov, P. Nokolić, Z. Tešanović, arXiv:1006.0447.
- <sup>24</sup> S. Graser, T. A. Maier, P. J. Hirschfeld, D. J. Scalapino, New J. Phys. **11**, 025016 (2009).
- <sup>25</sup> Fa Wang *et al.*, Phys. Rev. Lett. **102**, 047005 (2009).
- <sup>26</sup> C. Platt, C. Honerkamp, and Werner Hanke, New J. Phys. **11**, 055058 (2009). ; R. Thomale *et al.*, Phys. Rev. B **80**, 180505 (2009).
- <sup>27</sup> R. Thomale, C. Platt, W. Hanke, B. A. Bernevig, arXiv:1002.3599v1
- <sup>28</sup> A. V. Chubukov, M. G. Vavilov, A. B. Vorontsov, Phys. Rev. B **80**, 140515(R)(2009).
- <sup>29</sup> A. F. Kemper, T. A. Maier, S. Graser, H.-P. Cheng, P. J. Hirschfeld, and D. J. Scalapino, New J. Phys. **12**, 073030 (2010).
- <sup>30</sup> S. Graser, A. F. Kemper, T. A. Maier, H.-P. Cheng, P. J. Hirschfeld, and D. J. Scalapino, Phys. Rev. B **81**, 214503 (2010).
- <sup>31</sup> Y. Nakai, *et al.*, J. Phys. Soc. Jpn. **77**, 073701 (2008)
- <sup>32</sup> H.-J. Grafe, *et al.*, Phys. Rev. Lett. **101**, 047003 (2008)
- <sup>33</sup> Y. Wang, *et al.*, Supercond. Sci. Technol. **22** 015018(2009).
- <sup>34</sup> O. Millo, *et al.* Phys. Rev. B **78**, 092505 (2008)
- <sup>35</sup> J. D. Fletcher *et al.*, Phys. Rev. Lett., **102**, 147001(2009)
- <sup>36</sup> C. W. Hicks *et al.*, Phys. Rev. Lett., **103**, 177003(2009)
- <sup>37</sup> K. Hashimoto *et al.*, Phys. Rev. B **81**, 220501(R) (2010)
- <sup>38</sup> J.-Ph. Reid *et al.* Phys. Rev. B **82**, 064501 (2010).
- <sup>39</sup> Y. Nakai *et al* Phys. Rev. Lett. **105**, 107003 (2010).
- <sup>40</sup> R. T. Gordon *et al.* Phys. Rev. B **82**, 054507 (2010).
- <sup>41</sup> K. Hashimoto *et al.*, Phys. Rev. B **82**, 014526 (2010).
- <sup>42</sup> K. Hashimoto *et al.*, Phys. Rev. Lett. **102**, 017002 (2009)
- <sup>43</sup> L. Malone *et al.*, Phys. Rev. B **79**, 140501(R) (2009)
- <sup>44</sup> K. Nakayama *et al.*, arXiv:1009.4236 and references therein.
- <sup>45</sup> D. S. Inosov *et al.*, Phys. Rev. Lett. **104**, 187001 (2010).
- <sup>46</sup> Chang Liu *et al.*, arXiv:1011.0980 and references therein.
- <sup>47</sup> Seiichiro Onari and Hiroshi Kontani, Phys. Rev. Lett. **103**, 177001 (2009).
- <sup>48</sup> Z.-H. Liu *et al.*, arXiv:1008.3265.
- <sup>49</sup> W. L. McMillan, Phys. Rev. **167**, 331 (1968); N.N. Bogolubov, V.V. Tolmachev, and D.V. Shirkov, Consultants Bureau, 1959.
- <sup>50</sup> I. Mazin and J. Schmalian, Physica C, **469**, 614 (2009)
- <sup>51</sup> A. V. Chubukov Physica C **469**, 640(2009).
- <sup>52</sup> Daniel Podolsky, Hae-Young Kee, and Yong Baek Kim, Europhysics Letters **88**, 17004 (2009).
- <sup>53</sup> D. J. Singh, Phys. Rev. B, **78**, 094511(2008).
- <sup>54</sup> I. Aleiner *et al*, in preparation
- <sup>55</sup> J.F. Annett, N. Goldenfeld, and A.J. Leggett. JLTP **105**, 473 (1996).
- <sup>56</sup> P. Monthoux and D. Pines, Phys. Rev. B **49**, 4261 (1994); D.J. Scalapino, Phys. Rep. **250**, 329 (1995); Ar. Abanov, A. V. Chubukov, and M. R. Norman, Phys. Rev. B **78**, 220507 (2008).
- <sup>57</sup> I. Eremin and A.V. Chubukov, Phys. Rev. B **81**, 024511 (2010).
- <sup>58</sup> R. M. Fernandes and J. Schmalian, Phys. Rev. B **82**, 014521 (2010)
- <sup>59</sup> A.B.Vorontsov, M.G.Vavilov, and A.V.Chubukov, Phys. Rev. B **81**, 174538 (2010); M. G. Vavilov, A. V. Chubukov, and A. B. Vorontsov, Supercond. Sci. Technol. **23**, 054011 (2010).
- <sup>60</sup> K. Haule, unpublished.
- <sup>61</sup> Saurabh Maiti *et al*, unpublished.